FUJIFILM

ISSN : 0915-1478
CODEN : FFRDEK 59, 1-148 (2014)

FUJIFILM RESEARCH & DEVELOPMENT

No.59−2014

富士フイルム研究報告

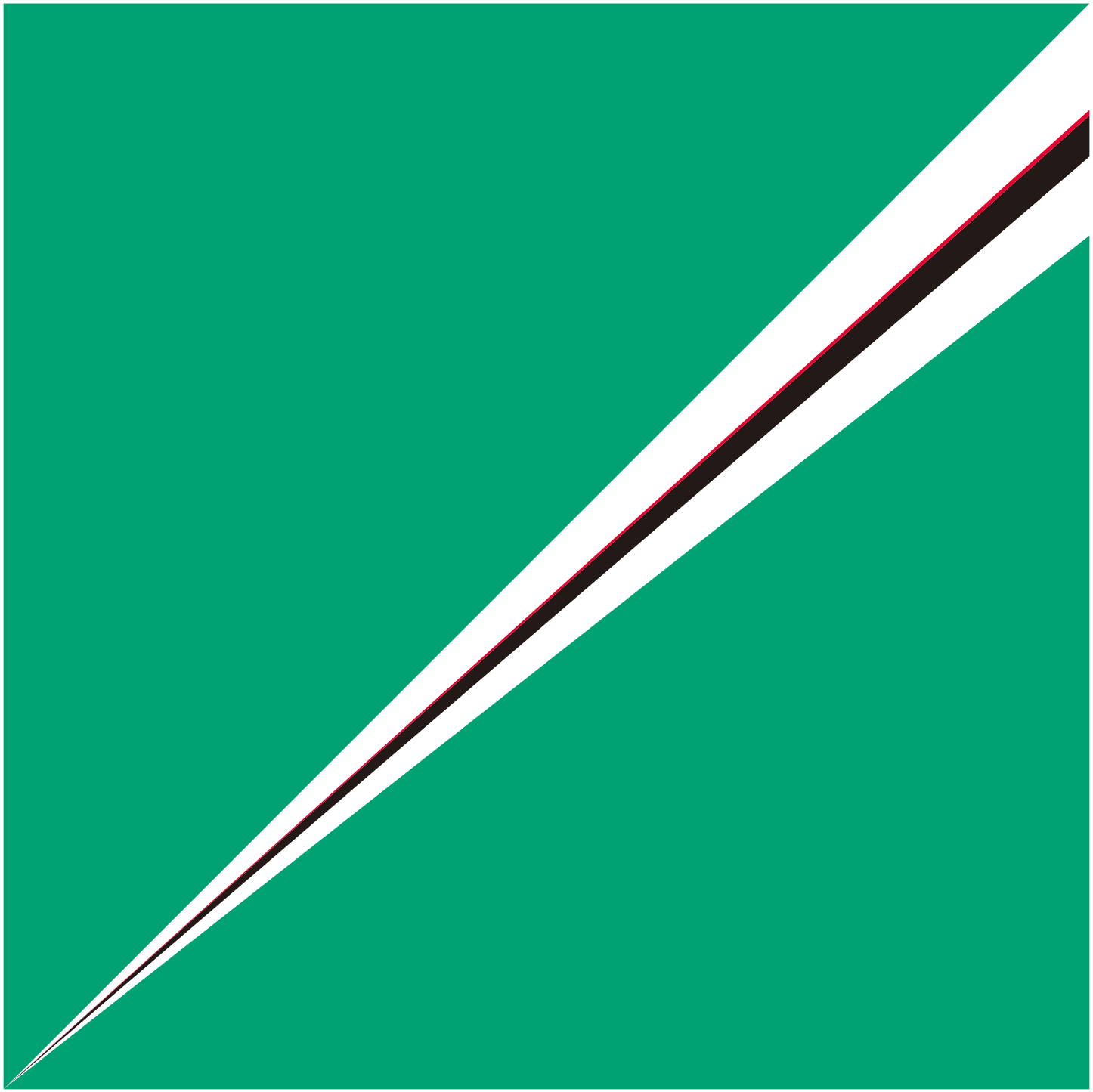

PURPOSE OF PUBLICATION

This annual publication is issued in order to introduce the results of research and development carried out in the laboratories of FUJIFILM Corporation and its subsidiaries. To provide an overview of our wide-ranging R&D activities across numerous business fields, this collection includes the papers, which are newly written or have already been published in various science and technology journals, regarding our noteworthy new products and novel technologies. In addition, a list of such papers published in journals and those presented at academic conferences in the past one year is attached at the end.

Published by Strategic Corporate Technology Planning Division,
Research & Development Management Headquarters,
FUJIFILM Corporation
Ushijima, Kaisei-machi, Ashigarakami-gun, Kanagawa 258-8577, Japan

Foreword

Masahiro Asami
Director, Corporate Vice President and
General Manager of the Research &
Development Management
Headquarters
FUJIFILM Corporation

On January 20, 2014, FUJIFILM Corporation celebrated its 80th anniversary. Since the establishment aiming the domestic production of photosensitive materials, during its long history of research for photosensitive materials and associated systems, the company has constantly introduced world-class products into the market. Furthermore, its research on non-silver salt photopolymers, magnetic materials and microcapsules has also led to many other excellent products. When the silver-halide photography market rapidly declined after the turn of the century, the company drastically diversified the scope of its research as well as its development objectives. Now, by applying core technologies developed based on our work on photosensitive materials, etc., we are releasing novel products into new fields such as high-functionality materials, digital printing and healthcare.

However, our conventional approach will no longer suffice to ensure further growth amid the changing world. To ensure decades of future prosperity, we will strive to create new value to society based on a new corporate slogan, "Value from Innovation". Our goal is to provide people with products and services that support their health and improve their quality of life, thereby creating more comfortable social environments. To that end, we must find out the true needs of our customers via interactive, co-creative processes with them and effectively utilize our technologies to provide new solutions to them.

In the future, instead of merely making incremental improvements in our conventional R&D, we must create substantial value by innovation based on technology combining other factors such as production systems, product lines and business models. To create innovation of true social value, we must review the objectives of our research, and think again how we conduct our development work.

The global economy is at last recovering from a prolonged slump. However, other social issues are becoming more serious: aging populations in combination with low birthrates and an unstable employment situation for younger generations in advanced countries, and the widening social inequalities in the process of development in emerging nations. Those factors will lead to major changes in corporate objectives and methods for creating social value. Accordingly, we need to clearly identify suitable targets for innovation, and then focus our R&D on them.

FUJIFILM Corporation will continue to bring innovation into society with its diverse products and services to support human health in the prevention, diagnosis and treatment of disease, make the environment greener and more sustainable, and allow people to live a more comfortable life.

This journal contains papers describing such research and development activities, and, I hope, it conveys the essence of our extensive R&D work. FUJIFILM Corporation will keep striving to achieve its mission of improving the future of humans and the earth through innovation.

FUJIFILM RESEARCH & DEVELOPMENT

No. 59

CONTENTS

Originals

* Co-researcher outside FUJIFILM Corporation

Development of Clinical Advanced Viewer "CA-V" for Supporting Clinical Practice

Takashi HOSHINO*, Shinichi TAKEYAMA*, Fumitake TANAKA*, Akinari TSUGO*, Yoshiyuki KURAMI*, Shoji KANADA*, and Akira OSAWA*

Abstract

We have developed the Clinical Advanced Viewer "CA-V" for supporting the clinical practice of physicians. The system can appropriately narrow down clinical information based on the problem, and can display the patient's information on a timeline on one screen. The physician can thus more easily diagnose and decide a treatment strategy, by referring to the aggregated clinical information of this system. The system is expected to enable physicians to more effectively understand the condition of a patient.

1. Introduction

In recent years, medical technology has become highly sophisticated, which has greatly increased the amount of information, such as examination images, sampling data, medication data and vital information.*1 Physicians need to refer to such information in their daily clinical activities to make a diagnosis of an individual patient or to decide his or her treatment plan.

In clinical practice, physicians select and carry out examinations according to the symptoms of the patient and, comparing the results with the past medical records, they identify changes in the patient's conditions, make diagnoses and consider treatment plans.

However, in cases when long-term follow-up observation is necessary or when the patient suffers from multiple diseases, the amount of data required for clinical practice becomes enormous and it takes much labor to collect and refer to them; therefore, a system has been requested that efficiently organizes and presents diverse information.

To respond to that demand, we developed the clinical advanced viewer CA-V.*2 The system narrows down, by patient and disease, the information required for physicians to make diagnoses or consider treatment plans, aggregates the time-series changes in the patient's conditions in a single window and thereby supports them with their clinical practice.

In addition to displaying diverse information after efficiently organizing it, the CA-V in conjunction with our medical-use image information system, SYNAPSE,*3 allows easy viewing of examination images. Moreover, in combination with our 3D image analysis system, Volume Analyzer SYNAPSE VINCENT, it is also possible to view the 3D image analysis results of examination images.

This report describes the clinical usefulness and system characteristics of the CA-V that we released via FUJIFILM Medical Co., Ltd. in July, 2013.

2. CA-V

This system provides two types of views: Time Line View (TLV) that visualizes and displays the clinical information of each patient as a graph on a timeline; and Time Slice View (TSV) that displays a table of numeric data for all the clinical information items. They can be selected depending on the current purpose. Our own database technology has enabled the quick display of the aggregated clinical information.

*1 Values and waveform information indicating the current conditions of the human body (pulse, heart rate, respiratory rate, blood pressure, body temperature, etc.)

*2 Acronym for Clinical Advanced Viewer

*3 The collective name for FUJIFILM radiology PACS (Picture Archiving and Communications System) products. The PACS is a medical-use image information system that electronically stores, retrieves and analyzes examination image data from medical-use image diagnosing systems such as CT, MRI and CR equipment.

Original paper (Received December 3, 2013)

*Medical System Research & Development center
Research & Development Management Headquarters
FUJIFILM Corporation
Miyanodai, Kaisei-machi, Ashigarakami-gun, Kanagawa
258-8538, Japan

2.1 Characteristics of the system

(1) Display of changes in the patient's conditions on a timeline in a single window

The TLV (Fig. 1) aggregates information required for clinical practice, such as basic information about the patient, examination images, sampling data, medication data and vital information, and instantaneously converts the data into a time-series graph in the window via simple user operations.

The display period can be changed via the intuitive operation of sliding the time scale setting bar. The graph can also be scaled up or down. That enables the easy, visual understanding of changes in the patient's conditions.

(2) Display of clinical information narrowed down by major disease using an original function

We have developed a smart function incorporating opinions from physicians, which allows the narrowing-down of clinical information items for each major disease. That streamlines the extraction process of data required for the disease from among enormous quantities of information.

(3) Display of a table containing numeric data for all the clinical information items

The TSV (Fig. 2) displays and enables easy reference of data of all the examination items without omission. In this view window, it is possible to check data even before the disease is identified, for example, at the first visit of the patient. After the identification of the disease, even when clinical information narrowed

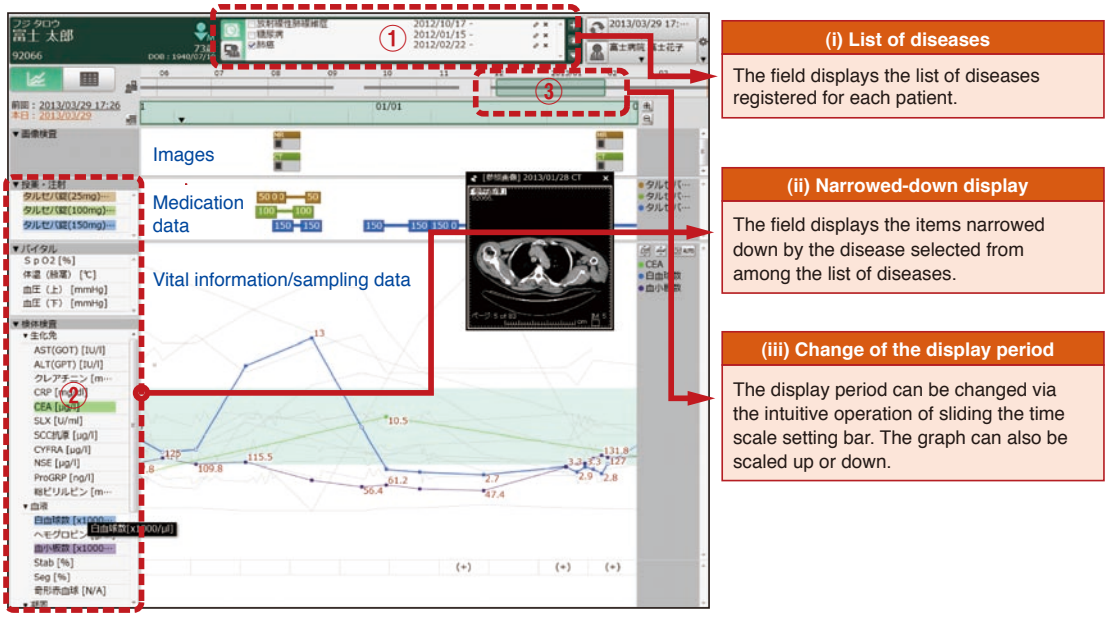

Fig. 1 Time Line View (TLV).

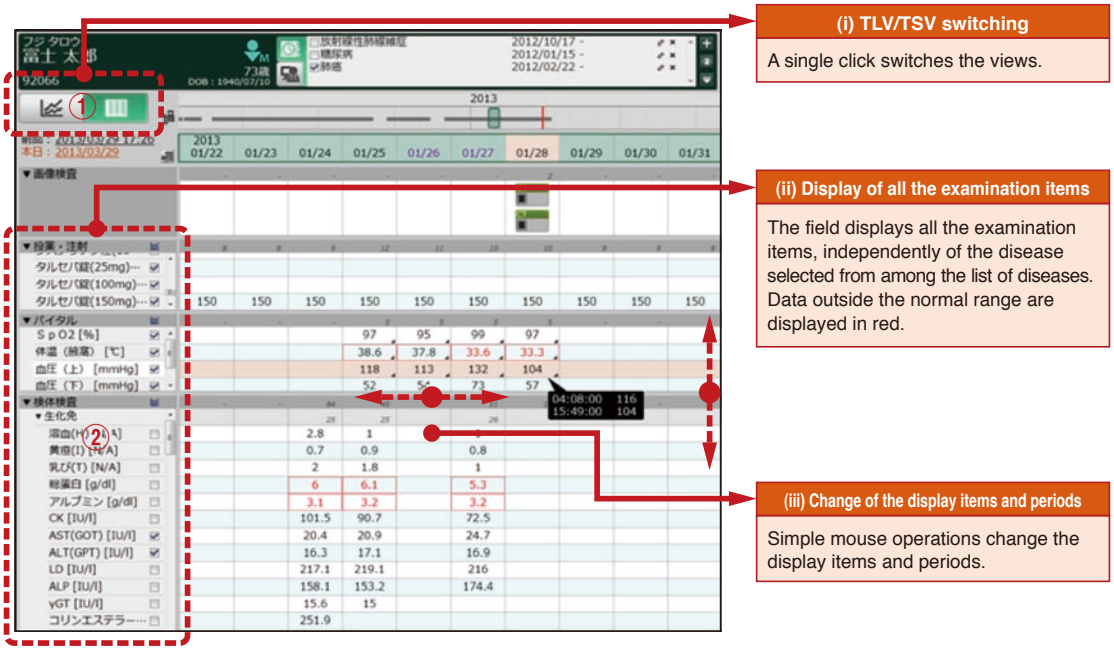

Fig. 2 Time Slice View (TSV).

down by disease is being referred to in the TLV, the window can be switched easily to the TSV, allowing the confirmation of numeric data of all the other clinical information items that are not displayed in the TLV.

(4) Linkage with SYNAPSE and VINCENT

Linking with SYNAPSE, the CA-V allows easy reference of examination images simply by setting the cursor over the target image icon. It can also display image diagnosis results in combination with our reporting system. Moreover, it is possible to view 3D image analysis results of SYNAPSE VINCENT from the CA-V.

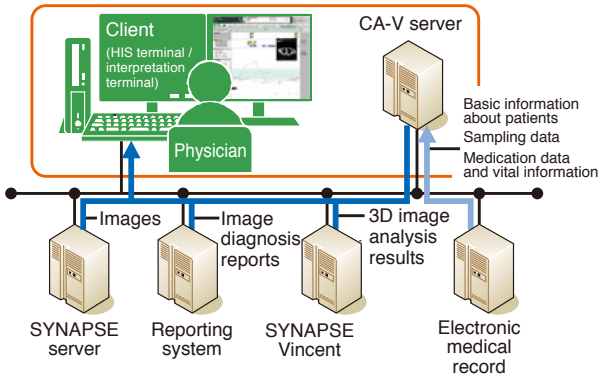

Fig. 3 Example of system configuration.

2.2 Configuration of the system

The system consists of a CA-V server and client terminals. The client terminals display clinical information using a web browser. The basic information about patients, sampling data, medication data and vital information are recieved from the Electronic medical record server. Fig. 3 illustrates a configuration example.

3. Database technology that enables high-speed display

Figs. 4 and 5 illustrate our original database technology that has realized high-speed data access. As shown in Fig. 4, this system does not recieved data as a set of all the necessary detailed information of each patient but creates purpose-specific summary tables (dimentions are data type and time : month · day), which enables rapid data reception.

In addition, as shown in Fig. 5, stratified reception of data required for display solves the issue of slow access observed in a conventional system when a large amount of clinical information is gathered in the case of longer treatment periods.

4. Product concept and value of the CA-V

The system was developed to visualize the clinical information and support physicians with their clinical decisions based on

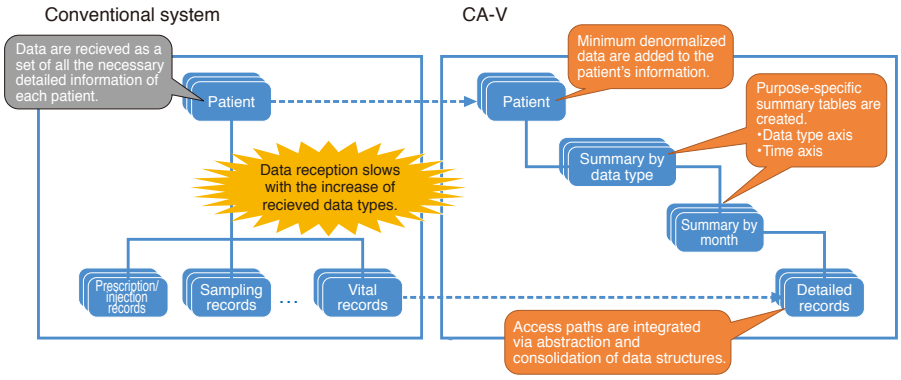

Fig. 4 Building a database summary for each object.

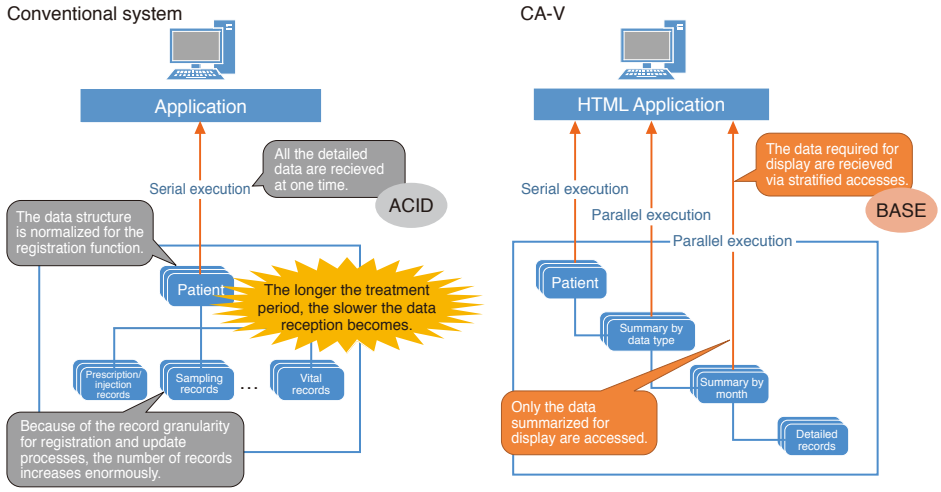

Fig. 5 Parallel data acquisition by BASE transaction.

the following concepts.

(i) Simple presentation of numerous types and enormous quantities of independently managed medical data
(ii) Pin-point reception of essential data
(iii) Visualization of important patterns and relations

It visualizes clinical information by displaying an aggregated item of values and graphs and their changes on a timeline.

4.1 Difference from conventional systems

(1) Issues of conventional systems

Current hospital information systems consist of several independent subsystems, such as the Electronic medical record system, examination system, nursing system and PACS, and the data are managed individually by the associated subsystems, for example, examination results by the examination system, nursing information by the nursing system and images by the PACS.

The main purpose of keeping Electronic medical record is to manage clinical descriptions as well as medication and examination orders; therefore, although being the primary tool to view a variety of data, they are not sufficient to display comprehensive data integrated from detailed records.

In the light of clinical practice, it is sufficient to view the examination results of a single day at the first visit of the patient but, when he or she is hospitalized, it is important to observe changes with time, comparing treatment and/or medication with the consequence (examination results) including side effects.

However, it is unrealistic to display all the raw medication and examination data on a timeline in a single window because the number of display items will then be enormous. In addition, such a volume of information will cause problems of system performance. Consequently, proper operability of Electronic medical record has not been realized.

(2) Solutions provided by the CA-V

The extent of medication and the role and importance of examinations vary depending on the patient. Sometimes, in addition to those to check the conditions of the current disease, examinations are carried out to detect other unexpected symptoms. In the former examinations, time-series display is useful while, in the latter, an indication of the results per examination may be good enough.

In medication, minor information, such as those about medicine for chronic maladies not directly related to the main disease and about intravenous infusions, is not necessary to confirm the condition of the treatment of the main disease.

That is, if the display items are limited to only those requiring the time-series confirmation of data essential for the clinical practice of the target disease, the number can be reduced greatly, which can fit into a single-window display.

We then developed and incorporated into the system a function in which users can display only essential data on a timeline by simply selecting the target disease according to the pre-defined display items for each disease (the "disease-specific display item set"). That has enabled physicians to easily refer the data of interest and to reduce the considerable amount of time and labor required to confirm the details.

Furthermore, by displaying medication data and examination results on a timeline, it has become possible to easily find the relationships between cause (treatment and/or medication) and effect (improvement and/or side effect). That allows physicians to concentrate on their original duties, clinical decisions and practice, without being bothered by the manipulation of tools.

4.2 Supported diseases of disease-specific view

We considered possible treatments and examination purposes for individual diseases according to clinical practice guidelines, etc.,[1)-12)] and incorporated into the system a definition file of items to be displayed on a timeline for each disease (disease-specific display item set). Currently, the display item set responds to about forty diseases (Table 1). It is available for use from the moment

Table 1 Supported diseases of disease-specific view.

	Respiratory organs	Circulatory organs	Digestive organs		Internal secretion
			Stomach and intestines	Liver, biliary tract and pancreas	
Cancer/tumor	Lung cancer		Stomach cancer Esophageal cancer Colorectal cancer GIST	Hepatic tumors Biliary tract cancer Pancreatic cancer	Thyroid cancer
Other major diseases	Lung infection COPD Interstitial pneumonia	Ischemic heart disease ・Angina pectoris ・Myocardial infarction Heart failure	Gastroduodenal ulcer Ulcerative colitis Crohn's disease	Hepatitis Cirrhosis Cholangitis/ cholelithiasis Pancreatitis	Diabetes

	Rheumatism/ collagen disease	Urinary organs	Breast oncology	Gynecology
Cancer/tumor		Kidney cancer Prostate cancer Bladder cancer Upper urinary tract cancer	Breast cancer	Cervical cancer Endometrial cancer Ovarian cancer Uterine fibroid
Other major diseases	Rheumatoid arthritis Other collagen diseases	Chronic kidney disease/ renal failure Dialysis		

the system is introduced to the site.

The disease-specific display item set is defined by broad categories of diseases. For example, lung cancer, lung infection, chronic obstructive pulmonary disease (COPD) and interstitial pneumonia are defined for respiratory organs, which can cover over 70 % of inpatients with respiratory disease.

The display item set covers major diseases, including lifestyle disease, as well as those requiring hospitalization for which examinations are essential.

Major diseases in the categories outside the scope of the current version will be supported as required in the next version onward.

4.3 Use of the TSV and TLV

(1) TSV

This view is designed to display the general data only around a specified date of medication and examinations performed on a patient for the confirmation of his or her condition at the first visit or unexpected symptoms in follow-up observation.

In general, Electronic medical records provide result data as a list per examination. Therefore, it is often difficult to identify the data of examinations rarely carried out if the dates are uncertain. However, this view displays a list of all the examination items, allowing easy reference of such rare data.

(2) TLV

The details of this view are illustrated in Fig. 6 below. The displayed information is not actual data but an example created for the purpose of explanation.

The list of diseases at the upper center of the window shows that this patient suffers from lung cancer and diabetes. Currently, "lung cancer" is selected and medication and examination data narrowed down by the disease are displayed. In cases where the patient has multiple diseases, selecting the checkbox for the target disease in this field displays the associated clinical data items.

The major medicines for lung cancer are anti-cancer, side-effect treatment and analgesic drugs. Analgesics are important only for advanced cancer; therefore, they are not displayed in the figure (the visibility is selectable). In this case, the first course of treatment was conducted with paclitaxel and carboplatin as anti-cancer drugs.

Examination items displayed are of vital signs (e.g., body temperature, pulse) to confirm the basic conditions of the patient, sampling data requiring caution to check for side effects of anti-cancer drugs and tumor markers to check the condition of cancer.

The figure shows a drop of the white blood cell count (WBC count), which is a typical side effect of anti-cancer drugs. When the count decreased to 900/μL, which was lower than the level that requires remedy (1000/μL), a treatment drug, Gran Syringe, was administered. It is clear at a glance that, as a result, the condition of the patient was improved. Consequently, in the second course, the dosage of anti-cancer drugs was reduced, considering side effects.

In addition, it is possible to view image data in the TLV. That allows easy confirmation of curative effects by comparing the sizes of tumors before and after anti-cancer therapy.

The above example is a case of a short-period display. The time scale can easily be changed as required. For example, it is possible to set a longer display period for image data and tumor marker information to about one year for follow-up observation after cancer therapy. Setting a long time scale enables the recognition of gradual changes in tumor markers that are not easily detected.

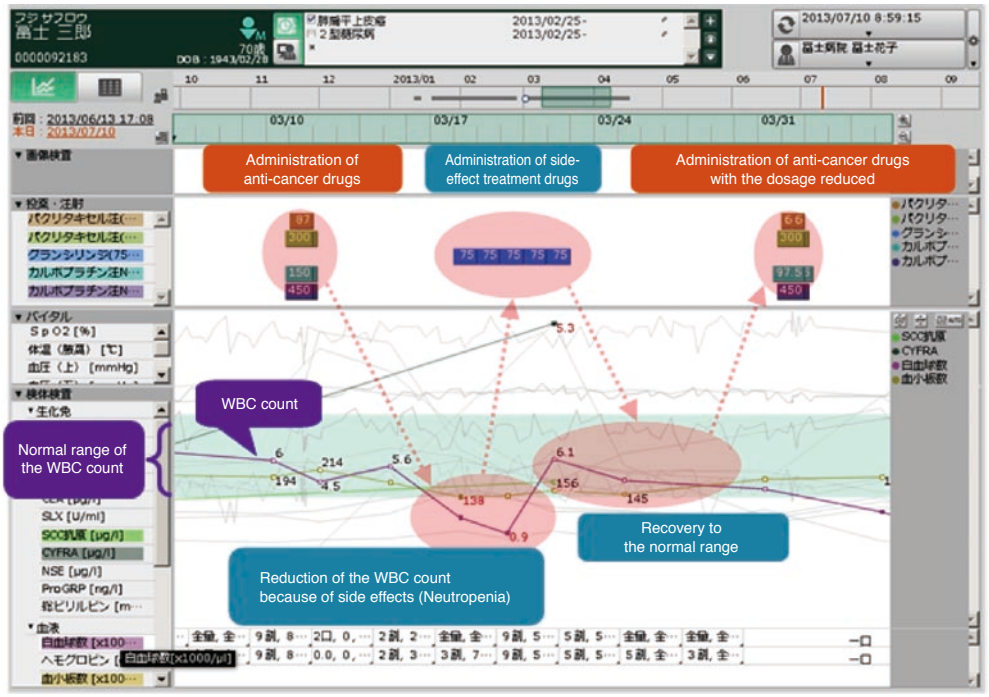

Fig. 6 Case of using Time Line View in clinical practice.

In reality, even after a diagnosis is made, the conditions of the disease vary depending on the individual patient and the confirmation of extra examination values may become necessary. In such cases, the display items of the TLV can be added via the TSV. The added items are saved together with the disease information of the patient. Therefore, next time the data of the same patient are referred, they are displayed in the TLV without setting again.

As described, the CA-V provides, via simple operations and in an easy-to-understand way, the information useful for a series of clinical processes such as the understanding of the contents of treatment, confirmation of its curative effects, recognition and treatment of any side effects, creation of new treatment plans and follow-up observation.

(3) Snapshot function

The timeline windows also display the summary of the course of important information for patients.

This system has a function that takes "snapshots" of the windows, saves and refers them at any time. It is expected that the function will be useful on various occasions, such as conferences, where physicians and health-care providers need to be involved in clinical practice, sharing the conditions of patients.

5. Conclusion

We developed the CA-V to efficiently provide optimal views of information at clinical sites where it is necessary to refer to enormous quantities of diverse clinical data and make decisions about diagnoses and treatment strategies based on them. The system thus aims to help physicians to make clinical judgments.

We are planning to add support functions and to further improve the information sharing function in the future.

We hope that the system will be introduced widely into clinical sites and will contribute to various clinical activities conducted there.

6. Acknowledgement

We express our special thanks to Kazuma Kishi, the Chief of the Department of Respiratory Medicine, Respiratory Center, Toranomon Hospital (Federation of National Public Service Personnel Mutual Aid Associations), and Atsuko Kurosaki, the Director of the Department of Diagnostic Radiology, Fukujuji Hospital (Japan Anti-Tuberculosis Association), who provided us with plentiful guidance in the development of this system.

References

1) The Committee for the Japanese Respiratory Society Guidelines in Management of Respiratory Infections. The Japanese Respiratory Society, "The Japanese Respiratory Society Guidelines for Management of Respiratory Infections". The Japanese Respiratory Society Guidelines for Management of Community-acquired Pneumonia. 2008, 72p.
2) The Japan Lung Cancer Society. Evidence-based Guidelines for Management of Lung Cancer 2005. Kanehara & Co.,Ltd., 2005, 191p.
3) Guidelines for the Diagnosis and Treatment of Cardiovascular Diseases(2009 JCS Joint Working Groups Report), Guidelines for the Treatment of Chronic Heart Failure(JCS2010). http://www.j-circ.or.jp/guideline/pdf/JCS2010_matsuzaki_h.pdf (reference,2014-02-14).
4) Guidelines for the Diagnosis and Treatment of Cardiovascular Diseases(2010 JCS Joint Working Groups Report), Guidelines for Treatment of Acute Heart Failure(JCS 2011). http://www.j-circ.or.jp/guideline/pdf/JCS2011_izumi_h.pdf (reference,2014-02-14).
5) The Japanese Society of Nephrology. Evidence-based Practice Guideline for the Treatment of Chronic Kidney Disease 2009. Tokyo Igakusha, 2009, 283p.
6) The Japan Society of Hepatology. Clinical Practice Guidelines for Hepatocellular Carcinoma 2009. Kanehara & Co., Ltd., 2009, 179p.
7) The Japanese Society of Gastroenterology. Clinical Practice Guidelines for Liver Cirrhosis. Nankodo Co., Ltd., 2010, 208p.
8) The Committee for Revision of the Pancreatic Cancer Medical Guideline. The Japan Pancreas Society. Pancreatic Cancer Medical Guideline 2009. Kanehara & Co., Ltd., 2009, 151p.
9) Publishing Committee of JPN Guidelines for Management of Acute Pancreatitis. JPN Guidelines for the Management of Acute Pancreatitis 2010. Kanehara & Co., Ltd., 2009, 160p.
10) The Japan Diabetes Society. Evidence-based Practice Guideline for the Treatment for Diabetes in Japan 2010. Nankodo Co., Ltd., 2010, 299p.
11) The Japanese Breast Cancer Society. Evidence-based Clinical Practice Guidelines of Breast Cancer 2011 for Treatment / Epidemiology and Diagnosis. Nankodo Co., Ltd., 2011.
12) Pharmaceutical and Food Safety Bureau, the Ministry of Health, Labour and Welfare of Japan. Guidance for the Proper Use of Narcotics in Medications: Guidance for the Use and Management of Opioid in Cancer Pain Management. 2012, 142p.

Trademarks

Development of Digital Mammography System "AMULET Innovality" for Examining Breast Cancer

Yoshinari ODA*, Takaaki ITO*, Keiichiro SATO*, and Junya MORITA**

Abstract

We have developed a new mammography system "AMULET Innovality" in which high image quality is achieved by a newly developed TFT panel with hexagonal close pattern structure. AMULET Innovality comes with dual tomosynthesis mammography modes for increased usability, to meet the various needs of different users. This report reviews the features of AMULET Innovality.

1. Introduction

In recent years, new technologies, such as digital breast tomosynthesis (DBT), have been introduced into the field of medical diagnosis and their use has been increasing at actual clinical sites.

Tomosynthesis is a technology to generate a tomographic image from multiple images taken so it can be utilized in diagnosis (Fig. 1). In addition to the creation of images at a high resolution, which has already been achieved in conventional mammography, tomosynthesis requires imaging at a lower radiation dose because examinees need to undergo mammography several times to make one tomographic image. To respond to those requirements, FUJIFILM developed a panel to achieve high image resolution and low radiation exposure for our new product, AMULET Innovality (Fig. 2).

AMULET Innovality provides two tomosynthesis mammography modes that are selectable depending on the purpose; imaging technology to achieve, with the low-radiation W anode, the same high-level of resolution as is possible with the Mo anode; and the intelligent auto exposure control function (i-AEC) to optimize the quality of images of the mammary gland region, regardless of the condition of the subjects such as having implants. The system was thus developed based on the consideration of its usability for patients, doctors and technicians.

This paper describes the main features of AMULET Innovality.

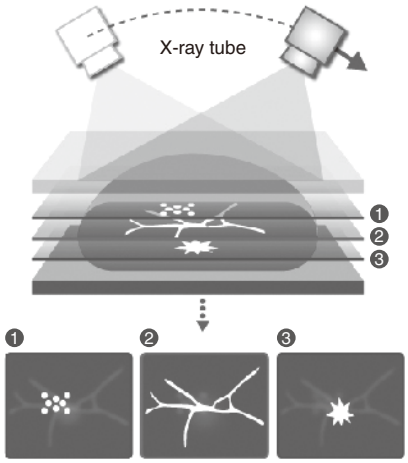

Fig. 1 Tomosynthesis Mammography.

Fig. 2 AMULET Innovality.

Original paper (Received December 3, 2013)

* Medical Systems Research & Development Center
Research & Development Management Headquarters
FUJIFILM Corporation
Miyanodai, Kaisei-machi, Ashigarakami-gun, Kanagawa 258-8538, Japan

** Imaging Technology Center
Research & Development Management Headquarters
FUJIFILM Corporation
Miyanodai, Kaisei-machi, Ashigarakami-gun, Kanagawa 258-8538, Japan

2. Main Features

2.1 HCP-structured TFT panel that achieves high resolution and low radiation exposure

We developed a panel that achieves high resolution and low radiation exposure by making design improvements to conventional TFTs.

The conventional design of TFTs incorporates spaces between neighboring picture elements (i.e., pixels) for the laying of signal wires and address wires. However, because those gaps do not have electrodes, the electrical field intensity is naturally weak there, which reduces the collection efficiency of signal charge generated from X-rays.

We then focused on the fact that, at the corners of square pixels constituting conventional TFTs, the electrical field is greatly disturbed and thus the collection efficiency of signal charge decreases significantly. Therefore, we introduced the hexagonal close pattern (HCP) structure into TFTs. With no sharp angles, hexagonal pixels can be arranged leaving no gaps, which suppresses the disturbance of the electrical field intensity at their corners. Consequently, we succeeded in increasing the sensitivity by about 20% compared with conventional TFTs using square pixels.

Fig. 3 illustrates the difference between the HCP structure of AMULET Innovality and the conventional structure consisting of square pixels and Fig. 4 shows their electrical field intensity dependent on the structural difference.

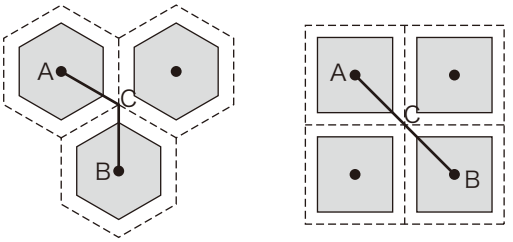

Fig. 3 Pixel form of HCP structure (left) and square pixels (right).

2.2 Two purpose-specific tomosynthesis mammography modes

In tomosynthesis, several breast images are taken from different angles to generate, via reconstruction, a tomographic image of the inside of the breast and the wider the imaging angle, the higher the depth resolution of the image becomes. Having directed our attention to that characteristic, we incorporated two different tomosynthesis mammography modes, i.e., ST mode and HR mode.

ST mode achieves imaging as quickly as just four seconds by narrowing the imaging angle. Also, the mode allows setting a low dose of radiation with auto exposure control (AEC), benefiting from the improvement of sensitivity gained via the introduction of the HCP structure. Quick and low-radiation tomosynthesis mammography is possible in this mode.

HR mode provides high depth resolution by widening the imaging angle. That enables observation focusing on the region of interest.

Fig. 5 presents conceptual diagrams for ST mode and HR mode, indicating the imaging angles and depth resolutions of their reconstructed images, respectively.

Providing those two distinctive modes allows users to make purpose-specific selection.

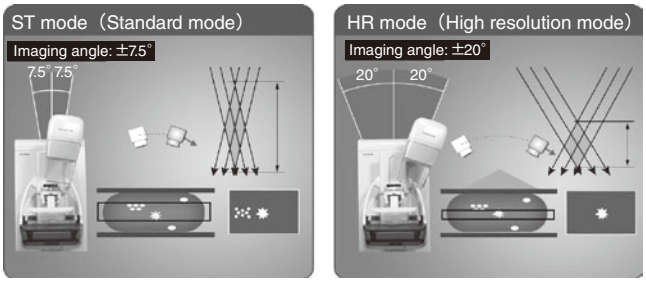

Fig. 5 Conceptual diagram of difference in reconstructed images due to different exposure modes.

2.3 Radiation quality correction that achieves the same quality of images with the W anode as with the Mo anode

In general, images taken with the Mo anode represent stronger contrast than with the W anode, which allows physicians to make diagnoses more easily.

X-rays generated from the Mo anode have a low energy distribution; therefore, they are easily absorbed in the breast. That enables high-contrast imaging. However, it also means that, with the Mo anode, the radiation dose is definitely larger than with the W anode.

We therefore addressed the difference in energy distribution between the two types of anodes and analyzed their radiation quality physically. As a result, we came to develop a radiation quality-correcting technology to create the same high quality of images with the low-radiation W anode as is possible with the Mo

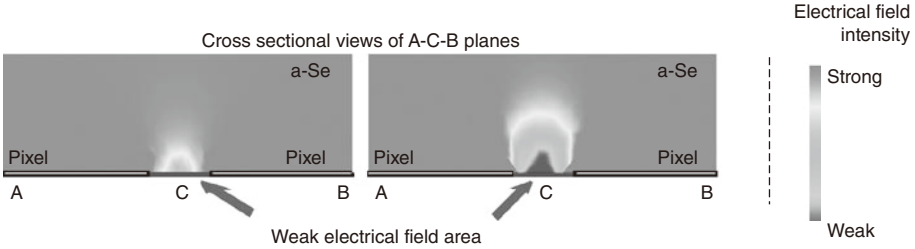

Fig. 4 Distribution of electric field intensity on A, B and C surface in Fig. 3.

anode: Image-based Spectrum Conversion (ISC).

Fig. 6 presents images taken, respectively, with the Mo anode (left) and with the W anode incorporating ISC (right). The images are of the same quality, while the radiation dose with the W anode was reduced by about 14% compared with the Mo anode.

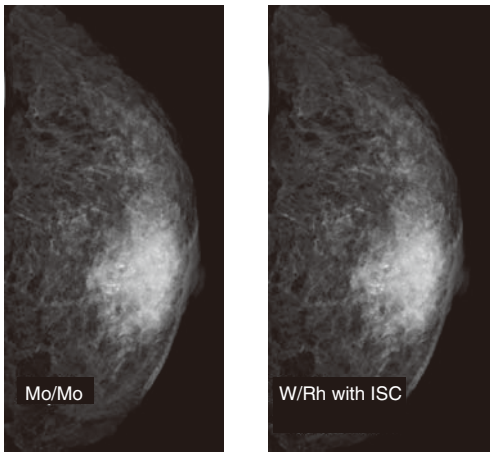

Fig. 6 Comparison of images exposed with Mo anode and with W anode & image processing.

2.4 i-AEC that achieves more precise radiation dose

We improved the conventional AEC function and incorporated that intelligent version, i-AEC, into AMULET Innovality.

The conventional AEC uses multiple sensors to detect X-rays that have passed through the subject. It calculates the required dose based on the sensor that received the smallest quantity of X-rays through the subject during pre-irradiation, that is, the sensor for the region where the glandular density is considered to be the highest. On the other hand, i-AEC detects the mammary gland region based on the morphological characteristics recognized within the images taken during pre-irradiation. The latter method has realized radiation dose control that optimizes the quality of images of the mammary gland region, regardless of the state of the breast, such as being fatty, with the scattered mammary gland and having implants.

Fig. 7 shows the results of the identification of the mammary gland region with i-AEC for multiple patients in different breast states. Regardless of the difference in condition, the region was localized precisely.

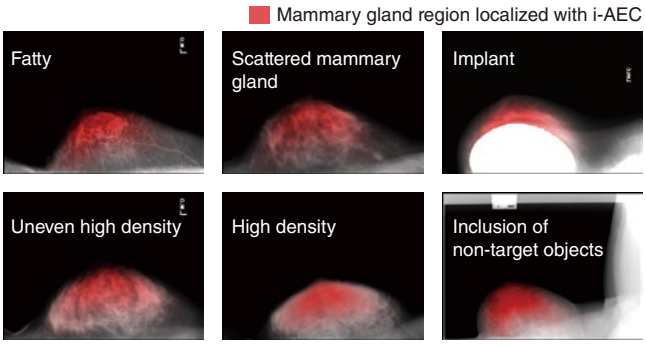

Fig. 7 Calculation result of mammary gland region in i-AEC.

3. Conclusion

This paper describes the main features of AMULET Innovality.

AMULET Innovality is not a mere mammography system incorporating a tomosynthesis function. It is the system of high total performance, excellent in both image quality and equipment usability. We expect that the system will contribute to the further development of diagnosis using mammography.

Trademarks

Technology for Improving the Sensitivity of an X-ray Automatic Detection Function "SmartSwitch"

Jun ENOMOTO* and Yasufumi ODA*

Abstract

In order to realize X-ray imaging in a patient room, we have developed a technology for improving sensitivity of X-ray automatic detection function "SmartSwitch". The main feature is the highly efficient scanning for X-ray signal and X-ray determination function. Due to the X-ray signal scanning efficiency, X-ray imaging with low power X-ray generator is possible. With SmartSwitch, it is possible to achieve both high X-ray detection sensitivity and prevention of false detection due to noise by X-ray determination function, and it can provide a user-friendly workflow.

1. Introduction

In the use of conventional flat panel detectors (FPDs), it is necessary to capture images in sync with X-ray generation by connecting the FPD controller to the X-ray generator with cables. However, many X-ray generators do not have interfaces to synchronize the timing with FPD controllers, which has prevented the replacement of computed radiography systems with FPDs.

Then, in 2011, we introduced onto the market for the first time in the world[1] the CALNEO *flex* incorporating an automatic X-ray detection function, SmartSwitch (Fig. 1). SmartSwitch captures images, detecting the start of X-ray irradiation with a cassette FPD; therefore, it does not require synchronization with X-ray generators. In recent years, however, there is an increasing demand for extending the usage of the cassette FPD from inside imaging rooms to the outside, such as during patient rounds and at home. To achieve that, X-ray generators must be changed from high-power types for imaging rooms to low-power types for use in mobile X-ray vehicles or portable equipment, requiring even higher sensitivity in X-ray detection.

This paper describes a technology, SmartSwitch, we developed to improve X-ray detection sensitivity.

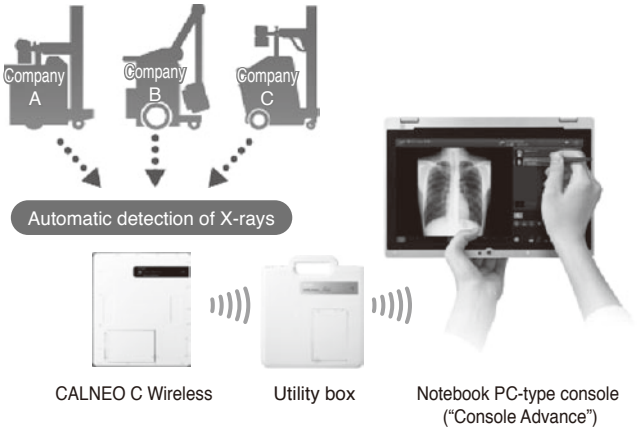

Fig. 1 System configuration of "CALNEO flex"

2. SmartSwitch technology to improve sensitivity

2.1 Outline of SmartSwitch

The cassette FPD sensor has a structure integrating a phosphor layer, which converts X-rays to light, and photodiode thin film transistors (TFTs), which convert the light to electrical signals. Imaging with a conventional X-ray generator connected requires changing the driving mode of the cassette FPD in the sequence, reset mode, image accumulation mode and image readout mode, in sync with X-ray irradiation timing via the cassette FPD controller (e.g., console).

On the other hand, imaging with the automatic X-ray detection function changes the driving mode of the cassette FPD upon detection of the start of X-ray irradiation. Instead of setting to reset mode, X-ray detection mode is started and, when X-rays are detected, the mode automatically changes to image accumulation mode (Fig. 2).

[1] Within wireless cassette digital radiography (DR) products on the market as of November 20, 2011 (an in-company investigation)

Original paper (Received December 5, 2013)

* Medical System Research & Development Center
Research & Development Management Headquarters
FUJIFILM Corporation
Miyanodai, Kaisei-machi, Ashigarakami-gun, Kanagawa
258-8538, Japan

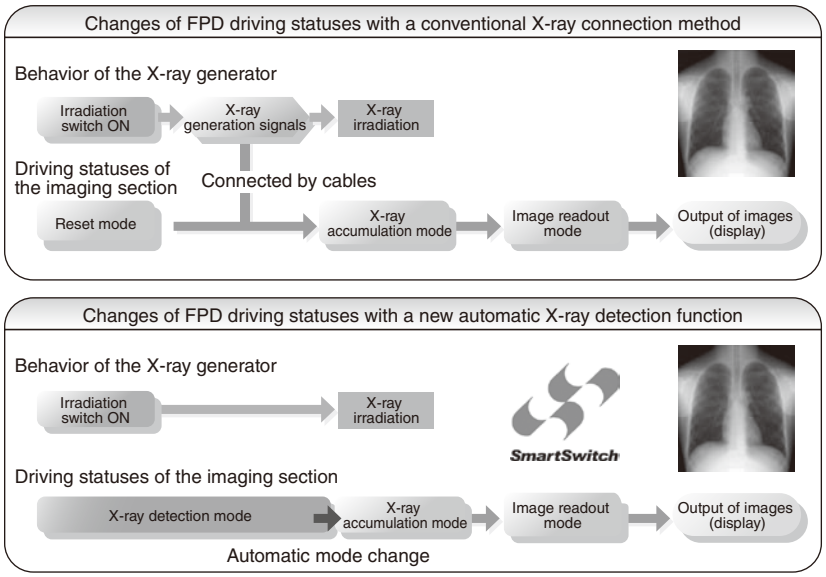

Fig. 2 Operational state of the X-ray detection system and automatic X-ray connection method

To improve X-ray detection sensitivity, we developed two algorithms for (i) the control of scanning to enable high-performance X-ray detection and (ii) the separation of noise from X-rays. The details are as follows.

2.2 Development of scanning control to enable high-performance X-ray detection

In X-ray detection mode, the following cycle is repeated at a high speed: integration and amplification of electrical charges to voltage with a charge amplifier; conversion to digital values with an A/D converter; and X-ray detection with a detection program. To improve the performance of X-ray detection, it is necessary to increase the proportion of the integral time for electrical charges. However, the conventional controller was connected to the cassette FPD as its external unit, requiring time for communication. In addition, the processing speed of the CPU was not sufficient for the parallel processing required.

To solve those issues, we have recently developed a dedicated control program and installed it into the processing IC within the cassette FPD. The communication time has thus been minimized. Moreover, we employed a field-programmable gate array (FPGA) for the processing IC, which enables it to perform real-time parallel processing.

2.3 Development of the X-ray determination function

In order for the automatic X-ray detection function to sense the start of X-ray irradiation and capture images, a quantity of X-rays not smaller than a threshold level should be irradiated onto the cassette FPD. The quantity of X-rays that reach the cassette FPD depends on the patient's physique and the output capacity of the X-ray generator. Accordingly, in imaging with a low-power X-ray generator for mobile X-ray vehicles or portable equipment,

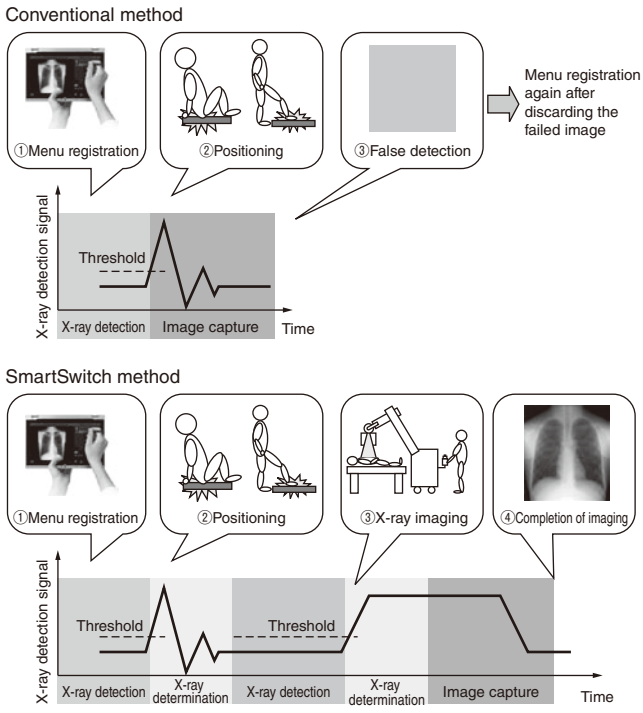

Fig. 3 Control of X-ray determination function

it is preferable that the threshold for X-ray signal detection should be set to a low value. However, that often causes false detection when the cassette FPD receives impacts from the patient's body motion or disturbance noise from peripheral equipment. That means, in general, there is a trade-off between X-ray detection sensitivity and the ability to prevent false detection.

To solve that issue, we developed an X-ray determination function to distinguish X-ray signals from noise when the signals exceed the threshold level. The function makes assessments on the signals when the driving status has changed from X-ray detec-

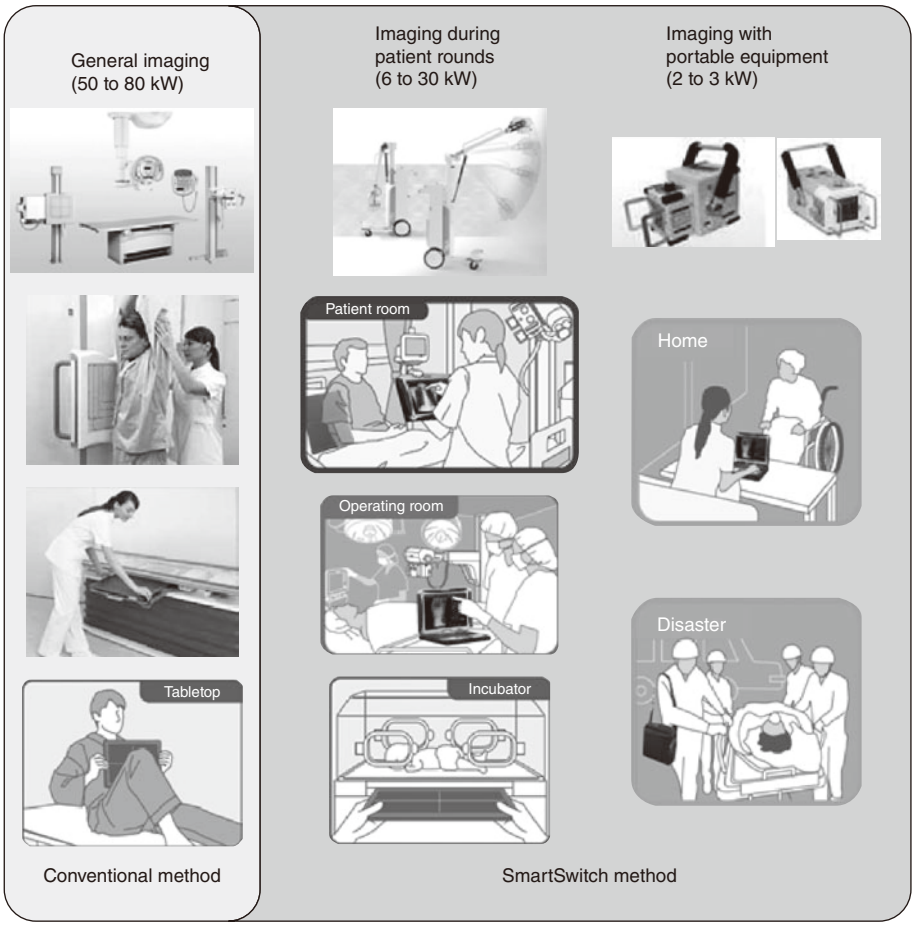

Fig. 4 Exposable situation of SmartSwitch

tion mode to X-ray accumulation mode with the scanned signals exceeding the threshold. If they are judged to be X-rays, the cassette FPD proceeds to imaging; otherwise, it is set back to X-ray detection mode without imaging the signals (Fig. 3). The function thus prevents false detection from impacts, etc., while keeping high X-ray detection sensitivity even if the quantity of X-rays that reach the cassette FPD is small.

3. Conclusion

Based on the sensitivity improving technology described in this paper, we put into use, for the first time in the world, the high-quality automatic X-ray detection function, SmartSwitch, that can be introduced easily even into existing low-power, analog mobile X-ray vehicles. The function is incorporated into all the CALNEO C-series panels, supporting a variety of imaging situations that require large panels (17 × 17 in.) such as in imaging rooms as well as small panels (24 × 30 cm) such as in incubators (Fig. 4). We will keep seeking to develop technologies to achieve the higher usability of DR imaging systems and to respond to needs at medical sites.

Trademarks

Development of Quantitative Immunoassay Reagent "FUJI DRI-CHEM IMMUNO AU Cartridge v-T4"

Tadahiro MATSUNO*, Tomoya OHARA*, Ayumi ONODA*, Kentaro NAKAMURA*,
Toshihito KIMURA**, and Akihiro KOMATSU**

Abstract

We successfully developed and commercialized "FUJI DRI-CHEM IMMUNO AU Cartridge v-T4" (FDC v-T4) and "FUJI DRI-CHEM IMMUNO AU10V", which is a quantitative immunoassay system for measurement of dog serum thyroxine (T_4). This system offers rapid measurement, simple operation, and a compact analyzer by using surface plasmonenhanced fluorescence (SPF) as the detection principle. Highly-precise T_4 inspection in veterinary clinics is possible by this system because the FDC v-T4 shows good correlation with the chemiluminescence enzyme immunoassay method which used by veterinarians via external orders.

1. Introduction

Thyroxine (T_4) is among the hormones secreted by the thyroid. Its blood concentration is controlled by interaction between the hypothalamus, hypophysis and thyroid as follows. Influenced by thyroid-stimulating hormone (TSH) secreted from the adenohypophysis, the thyroid increases T_4 secretion.[1), 2)] The adenohypophysis secretes TSH, stimulated by thyrotropin-releasing hormone (TRH) secreted from the hypothalamus. At the same time, the secretion of those hormones is inhibited via negative feedback that occurs upon an increase of the concentration of triiodothyronine (T_3) and T_4 in the blood. In that way, the secretion of the thyroid hormones is regulated (Fig. 1).

The diagnosis of hypothyroidism in dogs is based mainly on the measurement of dog serum T_4. When the thyroid function is impaired, the T_4 secretion that occurs upon stimulation by TSH is reduced. Therefore, it is known that many dogs suffering from hypothyroidism indicate a low serum T_4 concentration, while showing a high TSH value[3)].

In general, veterinary clinics entrust the T_4 test to external inspection organizations. That prevents veterinarians from promptly identifying the cause of the symptom because it takes time to get the results. In addition, pet owners must come back to the clinic for the confirmation of the results and for the treatment of their pets. Under such circumstances, there has been a demand for compact, rapid inspection systems that can be introduced into veterinary clinics.

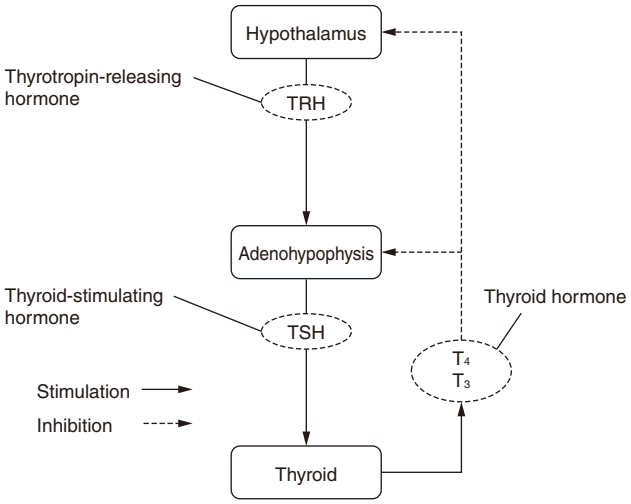

Fig. 1 Negative feedback mechanism for adjustment of thyroid hormones.

We therefore developed a compact quantitative immunoassay system that enables the measurement of dog serum T_4 at veterinary clinics and launched it onto the market in November, 2013. The system consists of a T_4 assay reagent cartridge, FUJI DRI-CHEM IMMUNO AU Cartridge v-T4 (hereinafter, the "FDC v-T4"), and the dedicated assay analyzer FUJI DRI-CHEM IMMUNO AU10V (Fig. 2).

Original paper (Received December 2, 2013)

* Pharmaceutical & Healthcare Research Laboratories
Research & Development Management Headquarters
FUJIFILM Corporation
Ushijima, Kaisei-Machi, Ashigarakami-gun, Kanagawa 258-8577, Japan

** Medical System Research & Development Center
Research & Development Management Headquarters
FUJIFILM Corporation
Miyanodai, Kaisei-Machi, Ashigarakami-gun, Kanagawa 258-8538, Japan

Fig. 2 Quantitative immunoassay system for measurement of dog serum T_4.

This is an immunoassay system utilizing an antigen-antibody reaction in which surface plasmon-enhanced fluorescence (SPF) was commercialized as its detection principle for the first time in the world. With this system, it has become possible to measure in vivo concentrations of small quantities of hormones without the intensive light or washing to reduce noise during measurement that are necessary with conventional methods. That realized the miniaturization of the system. In addition, because the time required for measurement is as short as approx. ten minutes, the results can be confirmed and explained to pet owners during their visits. The system is thus useful for precise diagnosis and treatment in the early stage.

This paper describes a detection technology established based on the fluorescent nanoparticle SPF method that is the fundamental of the system with the above features, together with the design of the FDC v-T4 immunoreaction cartridge utilizing the advantages of the SPF method and its clinical performance.

2. Development of the detection system

2.1 Surface plasmon-enhanced fluorescence method

When light is irradiated onto the thin metallic film formed on a transparent dielectric material, adjusting the incident angle to an optimal value (resonance angle) not smaller than the total reflection angle makes evanescent waves localized on the film resonate with compressional waves of free electrons (surface plasmons) there. Then, an enhanced photoelectric field is generated near the metal surface (near-field light). That phenomenon is called surface plasmon resonance (SPR). Surface plasmon-enhanced fluorescence (SPF) is a technology that detects fluorescence and measures the quantity of substances by intensely exciting, with the near-field light generated in SPR, fluorescent substances that exist near the metal surface. Among the characteristics of that technology are (i) signal amplification by the excitation light enhancing effect of SPR and (ii) noise reduction by local excitation near the metal surface using the near-field light. The synergy of those two features enables acquisition of very high S/N and improves sensitivity, compared with conventional detection methods using epifluorescence (Fig. 3).

In the academic domain, many studies on SPF technology have already been reported.[4), 5)] However, no industrial application cases had existed, because the SPF method has the problem of metal quenching that, if fluorescent substances get too close to the thin metallic film, excitation energy is retrieved by the film, which prevents its conversion to fluorescence. As a solution, a method has widely been taken in which metal quenching is inhibited by forming a preventive layer (dielectric layer) on the thin metallic film to ensure an appropriate space between the fluorescent substances and the surface of the film. However, that approach is not suitable for commercialization because it is not cost-competitive and the optimal layer thickness is difficult to design.[6), 7)] We therefore designed and developed original fluorescent nanoparticles including fluorescent substances in the quenching preventive layer and thus succeeded in solving the metal quenching problem (Fig. 4).

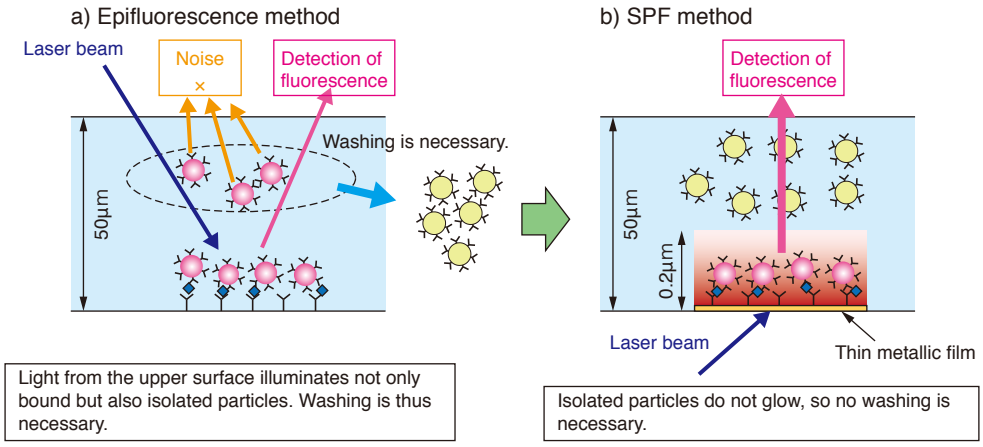

Fig. 3 Schematic drawings of a) epifluorescence method and b) SPF method.

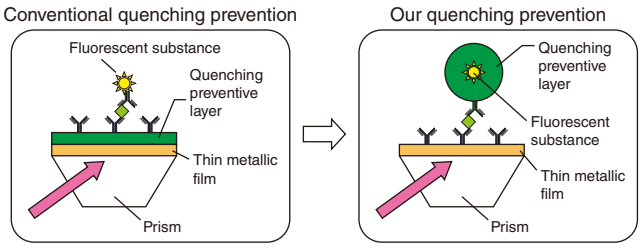

Fig. 4 Methods for preventing metal quenching.

Considering endurance against oxidization, we employed gold as the metal material. The results of comparison using fluorescent nanoparticles fixed onto the thin gold film confirmed that detection sensitivity with the SPF method is over ten times that with the epifluorescence method (Fig. 5).

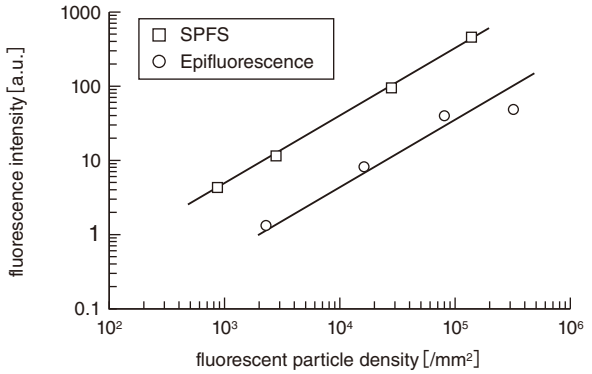

Fig. 5 Fluorescence intensity of SPF and that of epifluorescence method plotted against the number density of immobilized particles.

3. Development of the Immunoassay cartridge

3.1 Configuration of the cartridge

The FDC v-T4 immunoassay cartridge consists of a flow reaction plate and two cups (Fig. 6): Reaction Cup 1 containing a reagent (T_4 dissociation agent) that dissociates serum T_4 from T_4-binding protein; and Reaction Cup 2 containing anti-T_4 monoclonal antibodies that have been labeled using fluorescent nanoparticles (hereinafter, the "fluorescent particle-labeled anti-T_4 antibodies"). The reagent and the antibodies are sealed inside the cups respectively in dry form. The plate consists of a cover and a base having a thin gold film formed on a PMMA prism, and T_4-bound bovine serum albumin (T_4-BSA) is fixed on the film. By jointing this base with the cover, an immunoreaction channel with a height of approx. 50 μm is formed over the thin gold film.

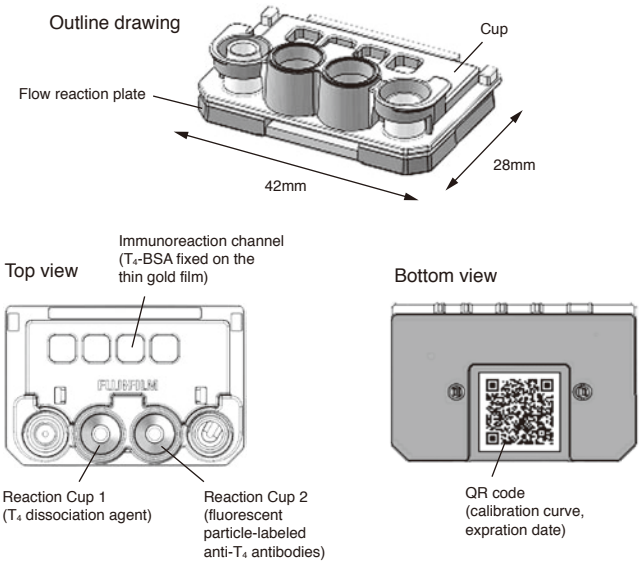

Fig. 6 Configuration of FDC v-T4 cartridge.

3.2 Reaction principle

T_4 is measured as follows (Fig. 7). First, a sample is dispensed into Reaction Cup 1 and T_4 is dissociated from T_4-binding protein (Step 1). Next, the reaction solution is dispensed into Reaction Cup 2 and fluorescent particle-labeled anti-T_4 antibodies react to T_4 contained in the sample, while dissolving in the solution (Step 2). During that time, as the serum T_4 concentration becomes higher, the quantity of T_4 bound to the antibodies on the fluorescent particles increases. That decreases the binding sites of the antibodies. Subsequently, the reaction solution is dispensed into the inlet of the reaction channel of the plate and, being sucked from the outlet side, it flows inside the channel. The fluorescent particle-labeled anti-T_4 antibodies that have not reacted to serum T_4 there react to T_4-BSA on the thin gold film, which causes the fluorescent particles to be captured near the film (Step 3). The reaction speed in Step 3 increases proportionally with the quantity of the binding sites of the antibodies on the fluorescent particles

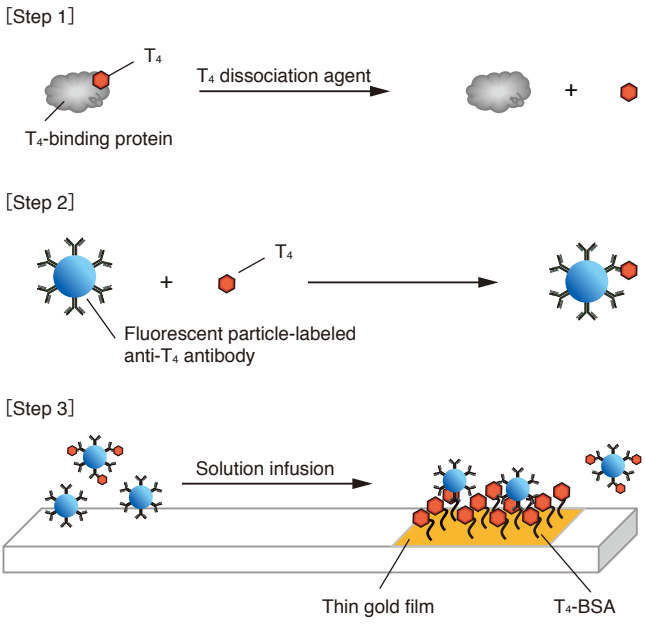

Fig. 7 Principle of measurement of dog serum T_4 by FDC v-T4.

and decreases inversely proportionally with the T_4 concentration of the sample. In the actual detection system, the time change of fluorescent signals (rate value) is obtained by exciting the fluorescent nanoparticles with a laser at the same time as the occurrence of the reaction in Step 3; the value is converted into the T_4 concentration based on the calibration curve information pre-recorded in the QR code attached onto the bottom of the cartridge; and the final measurement results are obtained.

The series of measurement actions described above (i.e., dispensing, mixing, solution infusion, detection and conversion to concentration) are performed automatically by the dedicated equipment and all measurers have to do for inspection is simply press the Start button after setting a sample, the cartridge and consumables.

3.3 Points of the development of the reaction system

(1) Design of the fluorescent nanoparticles

As previously described, we established a high-sensitivity fluorescence measurement method, having solved metal quenching by including fluorescent pigments in the quenching preventive layer. This paragraph describes the design of the fluorescent nanoparticles considering their application to immunoassays.

(i) Selection of the particle material

For the quenching preventive layer, it is possible to utilize light-transmitting materials, such as SiO_2 and polymers, which do not interfere with fluorescence. However, because of its ease in surface modification by antibodies and decentralized stabilization in the water system, we selected polystyrene ("PS") as the material.

For fluorescent substances to be included in PS particles, we selected a fluorescent pigment with an excitation wavelength of 660 nm and a fluorescence wavelength of 680 nm, taking into consideration the interference of serum samples with fluorescence (absorption and intrinsic fluorescence) and the versatility of the laser used in the photometric system.

(ii) Determination of the particle size

Particle sizes contribute to SPF excitation and immunoreaction differently. Therefore, to obtain highly sensitive and stable signals, it is important to select an optimal particle size, considering the contribution to both of them.

As regards SPF excitation, the larger the fluorescent particle diameter, the higher the excitation efficiency becomes. Because the SPR-enhanced photoelectric field decays exponentially in proportion to the distance from the surface, fluorescent pigments distant from the surface are difficult to excite. The reason is that the quantity of those pigments inside the particles increases proportionally with their volume; therefore, as a result, the fluorescence per particle increases (Fig. 8). On the other hand, considering immunoreaction, if the percentage by weight concentration of fluorescent particles is constant, the smaller the size, the higher the molar concentration becomes, which increases the reaction efficiency. Moreover, the fluorescent particles captured on the thin gold film by immunoreaction may decrease the reaction efficiency, having steric effects on the surrounding fluorescent particles. In such cases, too, small particle sizes act advantageously for the reaction efficiency. That is, because there is a trade-off relationship between the SPF excitation efficiency and the immunoreaction efficiency, particle size optimization is essential. We therefore performed simulation about the relationship between fluorescent particle sizes, immunoreaction efficiency and SPF excitation efficiency. The results revealed that a particle diameter between 150 and 400 nm can achieve efficient signals and the estimated optimal particle diameter was 250 nm (Fig. 9).

Based on the results of the above considerations, we developed original fluorescent nanoparticles and employed them in the reaction system of this immunoassay system.

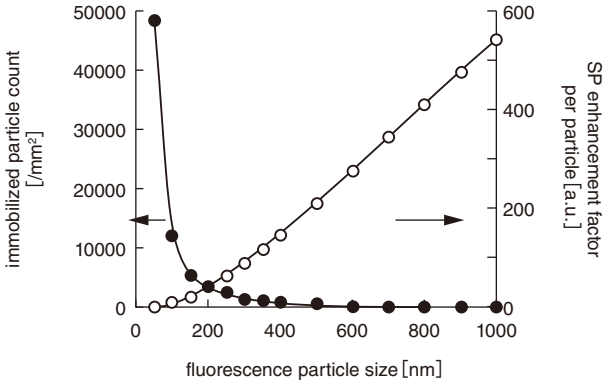

Fig. 8 Immobilized fluorescent particle count (solid circles, left scale) and SPF enhancement factor per particle (open circles, right scale) versus fluorescent particle size.

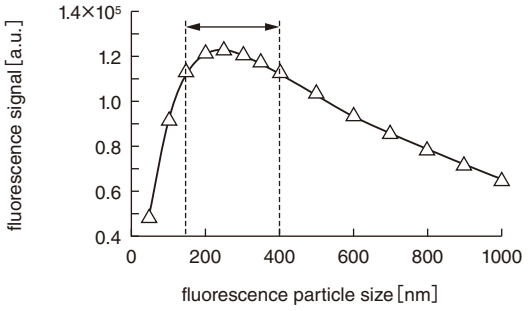

Fig. 9 Relationship between fluorescent particle size and signal strength obtained by SPF immunoassay. The arrow shows the optimal size range of fluorescent particles, 150-400nm, at 90% or more of the maximum fluorescence signal.

(2) Construction of the homogeneous assay system

In general immunoassays, a heterogeneous approach is employed in which unreacted labeled antibodies are removed after the antigen-antibody reaction via washing (B/F separation). How-

ever, it is not suitable for in-hospital inspection for the following reasons: (i) liquid waste is generated; (ii) measurement takes a long time because of B/F separation; and (iii) the measurement equipment is large. Because the SPF method employed in the FDC v-T4 has the advantage that only fluorescent labels near the thin gold film are excited, we were able to realize a homogeneous assay that does not need B/F separation.

As described in paragraph 3.2, fluorescent nanoparticles are captured on the thin gold film by supplying fluorescent particle-labeled anti-T_4 antibodies to the surface of the film with T_4-BSA fixed. During that time, by supplying the reaction solution inside the micro channel at a constant flow rate and thus preventing any decrease of the concentration of the sample near the reaction region (diffusion limitation), linear and more stable signals can be obtained in a short period without causing any decrease of the reaction speed. Fluorescent signals in SPF are affected to some extent by scattering caused by fluorescent nanoparticles on the surface of the thin gold layer. However, because the particle concentration is kept stable by the constant supply of reaction solution, the effect of scattering does not change with time and the intended antigen-antibody reaction rate is unaffected (Fig. 10). The introduction of the rate approach into the measurement method has thus enabled the extraction of only the target signals without washing via B/F separation. We not only realized short measurement times but also succeeded in the size reduction of the equipment.

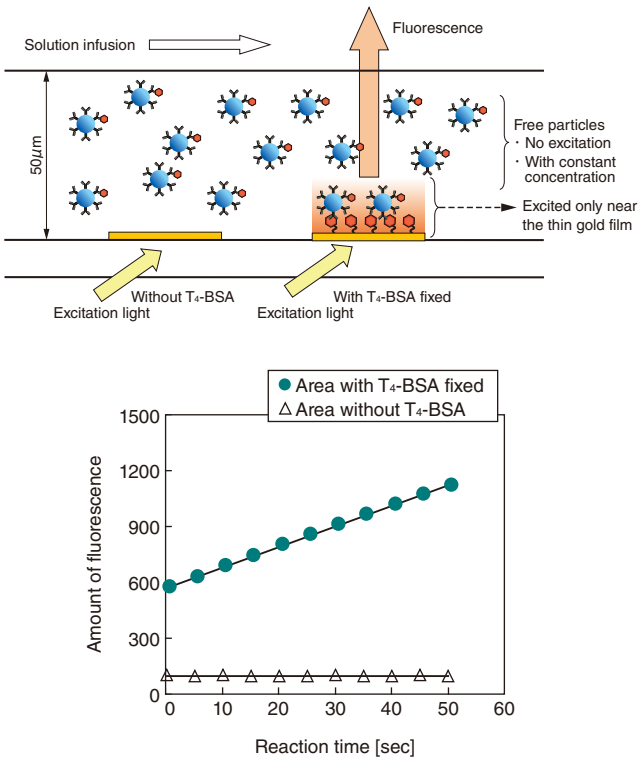

Fig. 10 Homogeneous immunoassay by SPF-rate method.

(3) Inhibition of the agglutination of fluorescent nanoparticles

In performing immunoreaction in serum using fluorescent nanoparticles as labels, a problem was observed that reactivity was much lower than in buffer solution because particle agglutination occurred. To solve it, we added, as a pre-treatment reagent, high-concentration magnesium chloride to the serum to inhibit the agglutination of fluorescent nanoparticles and thus improved the reactivity. That enabled measurement without diluting samples (Photo 1).

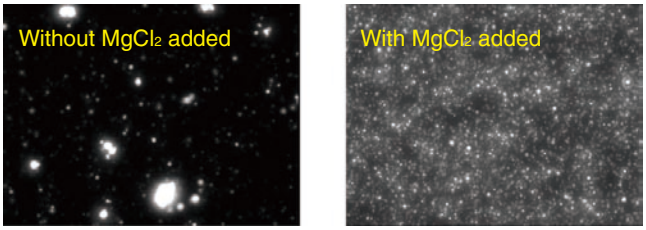

Photo 1 Improvement of particle dispersibility in serum with magnesium chloride.

4. Clinical performance of the FDC v-T4

4.1 Confirmation of correlation

To verify the effectiveness of the FDC v-T4, we confirmed correlation in dog serum, using as a control method the chemiluminescence enzyme immunoassay[8] (CLEIA) method employed by veterinary inspection centers.

The FDC v-T4, with a correlation coefficient (r) of 0.958, indicated a good correlation with the CLEIA method. Slope (a) and intercept (b) of the regression line (y=ax + b; x for the CLEIA method, y for the FDC v-T4) were 0.972 and −0.116 respectively, which confirmed that the measured T_4 values for the FDC v-T4 were very close to those for the CLEIA method (Fig. 11). That is, the FDC v-T4 enables a very quick in-hospital inspection that is as precise as those available at external inspections.

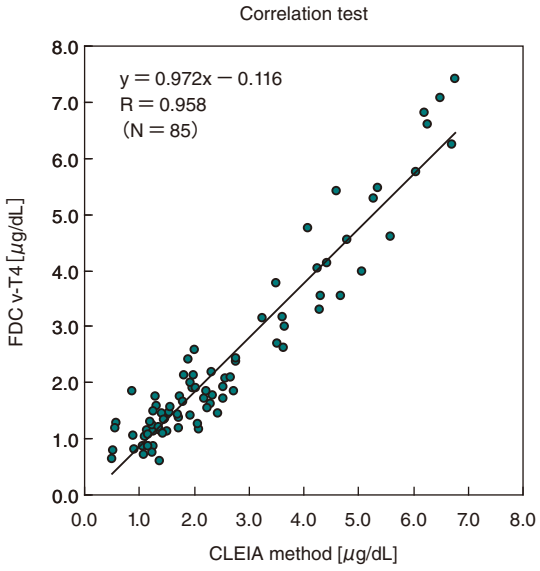

Fig. 11 Correlation between CLEIA method and FDC v-T4.

4.2 Confirmation of simultaneous reproducibility

We performed measurement on the same sample repeatedly with the FDC v-T4 and checked its simultaneous reproducibility. Table 1 shows the results of measurements performed ten times each using three test solutions with different T_4 concentrations. At each concentration level, the coefficient of variation (CV), which is a criterion for variation, was 6% or less. The results confirmed that the reagent used has sufficiently high reproducibility (quantitativity) for immunoassays.

Table 1 Reproducibility of measurements with FDC v-T4.

T_4 level	Low	Middle	High
1	1.26	4.24	6.01
2	1.08	4.29	6.13
3	1.24	4.34	6.15
4	1.25	4.41	6.00
5	1.20	4.44	6.40
6	1.20	4.37	6.41
7	1.21	4.16	6.49
8	1.06	4.50	6.31
9	1.15	4.11	6.13
10	1.13	3.95	6.78
Ave. (μg/dL)	1.18	4.28	6.28
SD (μg/dL)	0.07	0.17	0.18
CV (%)	5.9	4.0	2.9

(μg/dL)

5. Conclusion

We developed a quantitative immunoassay system for animals, FUJI DRI-CHEM IMMUNO AU Cartridge v-T4, and the dedicated assay apparatus, FUJI DRI-CHEM IMMUNO AU10V. By employing SPF as its detection principle, we realized a compact system design without the washing process that is necessary for general immunoassay systems, enabling quick and easy T_4 inspection inside veterinary clinics. Although it is a desktop inspection apparatus, the system exhibits high correlation with the CLEIA method used by external inspection organizations. Therefore, it can be said that the system provides high-precision inspection results.

We have an extensive product lineup in the veterinary clinic market, such as biochemical examination systems, digital X-ray image diagnosis systems and ultrasound equipment and they have been introduced into many facilities. In the future, based on this system as a platform, we are going to promote our research and development activities in the field of immunoassay, extending measurement subjects beyond T_4, and to thereby contribute to further improvement of the quality of medical care for animals.

6. Acknowledgement

We express our special thanks to the members of the Production Engineering & Development Center who exerted themselves for the design and development of this cartridge, as well as those in the Imaging Materials Production Division and FUJIFILM Photo Manufacturing Co., Ltd., who made great efforts to construct the reagent manufacturing system for the commercialization of the cartridge.

References

1) Reimers, T. J. ; Lawler, D. F. ; Sutaria, P. M. ; Correa, M. T. ; Erb, N. Effects of age, sex, and body size on serum concentrations of thyroid and adrenocotical hormones in dogs. American Journal of Veterinary Research. **51** (3), p.454-457 (1990)

2) Masuda, K.; Miyabayashi, T. Syodobutu Rinsho(Japanese Journal of Small Animal Practice). **15** (4), 57-62 (1996)

3) Ward, C. R. Inu To Neko No Kozyosen(The Thyroid, Saunders Veterinary Clinics, Small Animal Practice). Naoaki Matsuki, trans. Interzoo Publishing Co., Ltd. 2008, 190p.

4) Yu, F. ; Yao, D. ; Knoll, W. Surface Plasmon Field- Enhanced Fluorescence Spectroscopy Studies of the Interaction between an Antibody and Its Surface- Coupled Antigen. Analytical Chemistry. **75** (11), p.2611-2617 (2003)

5) Arima, Y. ; Teramura, Y. ; Takiguchi, H. ; Kawano, K. ; Kotera, H. ; Iwata, H. Surface plasmon resonance and surface plasmon field-enhanced fluorescence spectroscopy for sensitive detection of tumor markers. Methods in Molecular Biology. **503**, p.3-20 (2009)

6) Naya, M.; Tomaru, Y.; Horii, K. High-sensitive Biosensor Using Plasmon Resonance. Oyo Buturi. **80** (9), p. 808-812 (2011)

7) Horii, K. ; Kimura, T. ; Ohtsuka, H. ; Kasagi, N. ; Oohara, T. ; Matsuno, T. ; Hakamata, M. ; Komatsu, A. ; Sendai, T. Proceeding of SPIE, **8234**, 82340V (2012)

8) Kayama, T.; Arakawa, M.; Tsuchiya, R.; Nakase, Y.; Yajima, T.; Kita, H.; Higaki, K.; Adachi, H.; Hisasue, M.; Ogata, M.; Yamada, T. Program/Proceeding of the 1st JCVIM General Meeting. The Japanese College of Veterinary Internal Medicine. 2004, A-21.

Trademarks

Development of Cosmetics Brand for Pimples “Lunamer AC”

Makiko AIMI*, Yuki IMAIZUMI*, Akina NAKAUNE*, Noriko OHIRA*, Takuji KOSUGI*,
Naoko YOSHIDA***, Eriko IKENAGA***, Takeharu TANI***, and Gen OMURA****

Abstract

“Adult pimples” are serious skin trouble for women in their 20s and 30s. By using our original image analysis technology, we have found that the major cause of adult pimples is not the amount of oil but a partial drying state of the skin. We have developed a unique new ingredient “Acne shooter” which is 80 nm in diameter. Acne Shooter is a nano capsule made from stearyl glycyrrhetinate (active ingredient for acne) and natural vitamin E, glycerin (moisturizer). We confirmed that Acne shooter infiltrates into pores intensively, increases the moisture level of the skin, and improves the water-retaining function inside the skin. Based on this invention, we have developed “Lunamer AC” containing this new Acne shooter ingredient to reduce adult pimples.

1. Introduction

In addition to the research on collagen we have pursued for over eighty years, we have introduced our antioxidation and nanosization technologies into the research and development of FUJIFILM healthcare products, including the ASTALIFT brand.

The Lunamer series are basic skin care products to solve skin problems, targeting women in their 20s and 30s. The Lunamer AC (acne care) series (Fig. 1) launched onto the market in September, 2013, was developed to reduce adult pimples. Having identified their cause via our original skin analysis technique, we created a new ingredient named Acne Shooter that infiltrates intensively into pores where pimples grow and we have blended it into our cosmetics products.

2. Adult pimples

The principal cause of pimples has been thought to be the clogging of pores with oily matter and the consequent inflammation nearby due to excessive sebum secretion. In the case of pimples in puberty, the factor causing the excessive sebum secretion is said to be the activation of the male hormone. On the other hand, the causes of pimples in grown-ups, whose sebum should have decreased, are considered to be the changes in its secretion due to disorders in hormone balance related to menstrual cycles or daily stress, etc., or its increase to protect dry skin. However, the definite mechanism was yet to be identified.

Fig. 1 New cosmetic brand “Lunamer AC”.

Original paper (Received December 3, 2013)

* Pharmaceutical & Healthcare Research Laboratories
Research & Development Management Headquarters
FUJIFILM Corporation
Ushijima, Kaisei-machi, Ashigarakami-gun, Kanagawa
258-8577, Japan

** Imaging Technology Center
Research & Development Management Headquarters
FUJIFILM Corporation
Miyanodai, Kaisei-machi, Ashigarakami-gun, Kanagawa
258-8538, Japan

*** Frontier Core-Technology Laboratories
Research & Development Management Headquarters
FUJIFILM Corporation
Ushijima, Kaisei-machi, Ashigarakami-gun, Kanagawa
258-8577, Japan

**** Analysis Technology Center
Research & Development Management Headquarters
FUJIFILM Corporation
Nakanuma, Minamiashigara, Kanagawa
250-0193, Japan

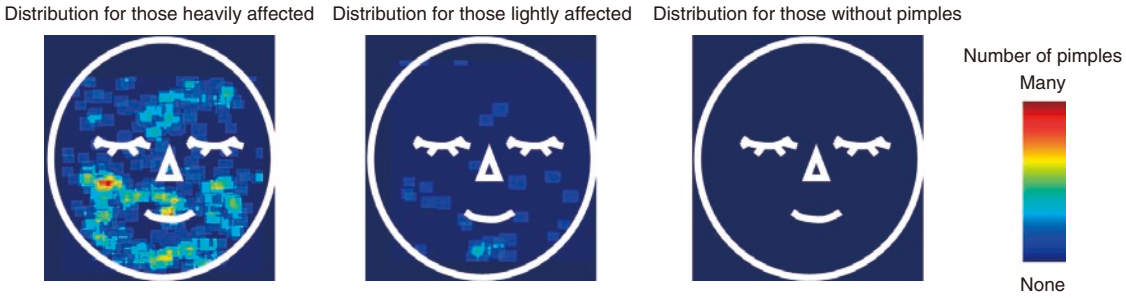

Fig. 2 Pimple points in the whole face.

3. Identification of the cause of adult pimples using the original skin analysis technique

3.1 Visualization of pimple regions

Dark spots, wrinkles, pores and pimples of the skin all have a variety of colors and shapes. Using a technology that analyzes, from images, the individual characteristics of their colors, shapes and regions, we precisely localized reddish, inflammatory pimples in the face images of twenty-five women in their 20s and 30s. We then categorized them into three groups, i.e., those heavily affected (having at least fifteen pimples); those lightly affected; and those without pimples, according to which, we visualized regions where pimples tend to grow on the whole face by superimposing all those images (Fig. 2).

The visualization results revealed that pimples grow frequently and intensively on the lower part of the face, in particular, along the face line. Also it was indicated that those lightly affected tend to have pimples locally on their chin.

3.2 Correlation of the amount of moisture and oil content with pimple regions

With twelve women in their 20s and 30s, we performed multi-point measurement (five points along the face line and nine points of other parts of the face) of the amount of facial moisture and oil content after they washed their faces and their skin stabilized in an environment at a room temperature of 23°C and a humidity of 50%. We then analyzed correlation between those two factors and pimple regions.

Fig. 3 shows facial moisture distributions. According to the figure, those heavily affected by pimples had partially dry skin with little moisture, in particular, along the face line, and those lightly affected had locally dry skin at a part of the forehead or chin. Those without pimples had homogeneous facial skin moisture and no dry parts observed. Regardless of pimples, there was no significant difference in the amount of their facial oil content.

The correlation*1 of the moisture ratio of the face line to the rest of the face with the number of pimples revealed a tendency for pimples to increase as the difference between the amounts of moisture in those two regions becomes larger.

As regards the oil content ratio, no correlation*1 with pimples was observed.

We also analyzed the relationship of the amounts of facial moisture and oil content with menstrual cycles. Those who tend to grow pimples before menstruation have obvious, partially dry skin then, while the others exhibit few changes in facial moisture before and after menstruation.

4. Acne care utilizing pores

For efficient adult pimple treatment, it is essential to resolve the above described "partially dry" condition, that is, to intensively moisturize partially or locally dry facial areas, as well as to precisely administer anti-inflammatory ingredients into pores where pimples are growing.

Pores have sebaceous glands as appendages. They are naturally oily, and water-soluble ingredients do not easily infiltrate into them. Therefore, we considered that highly lipophilic, oil-soluble, anti-inflammatory ingredients would be effective for smooth absorption into the pores.

4.1 Development of Acne Shooter

Stearyl glycyrrhetinate is an oil-soluble, natural plant-derived ingredient that is extracted from a bean-family perennial, licorice. It is known to have anti-inflammatory and anti-allergic effects. Among oil-soluble, anti-inflammatory active ingredients*2 that are approved for blending into cosmetics in Japan, it is the most highly lipophilic and, because of its high crystallinity, it does not easily dissolve in water, which has prevented it from being blended into cosmetics effectively.

Under such circumstances, we succeeded, with our original nanosization technology, in stably nanosizing such stearyl glycyrrhetinate into 80-nm particles combining other moisturizing ingredients and thus created a new acne care ingredient, Acne Shooter, that allows for effective introduction into cosmetics (Figs. 4 and 5).

*1 Correlation: Relation between $\frac{\text{Average amount of moisture (oil content) of the face line}}{\text{Average amount of moisture (oil content) of the rest of the face}}$ and the number of pimples

*2 Anti-inflammatory active ingredients that the Ministry of Health, Labour and Welfare of Japan has permitted to be blended into cosmetics (as of the end of June, 2013)

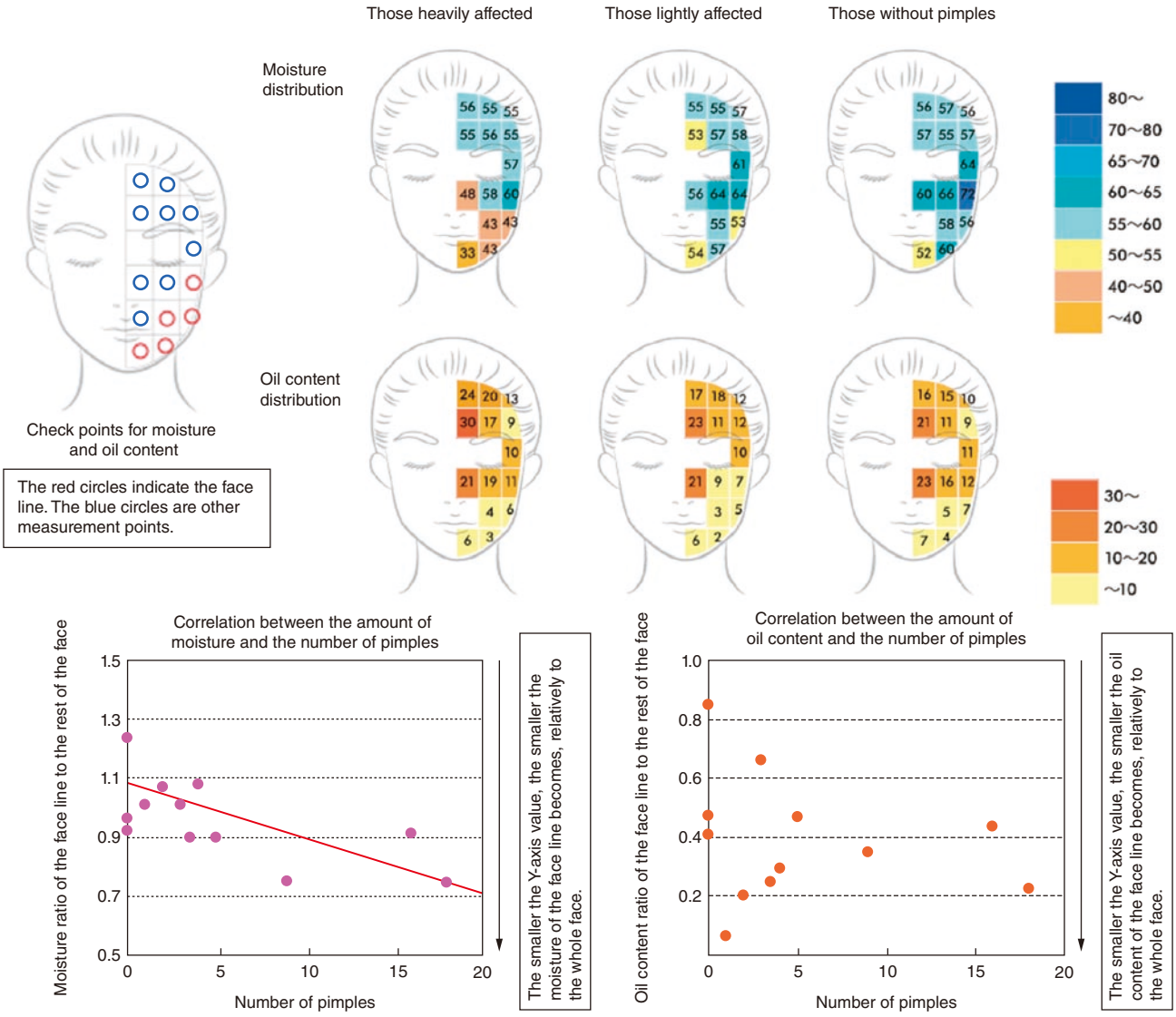

Fig. 3 Amount of moisture and oil content in the whole face.

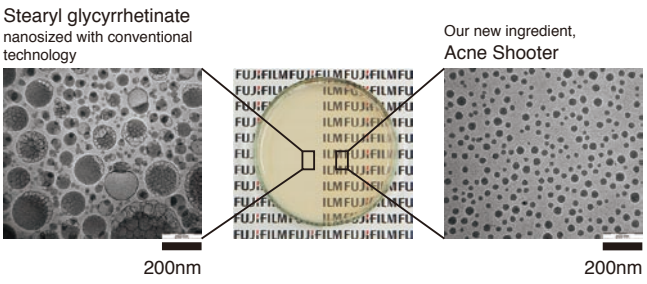

Fig. 4 TEM images of stearyl glycyrrhetinate dispersion.

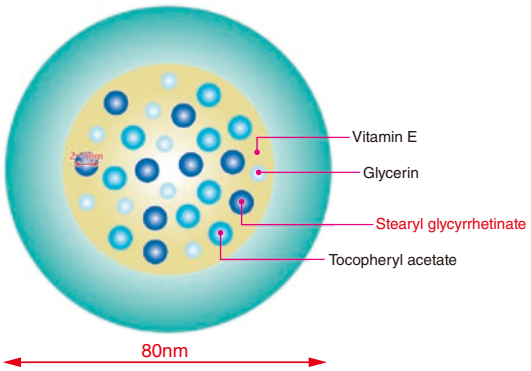

Fig. 5 Image of “Acne shooter”.

4.2 Intensive infiltration of Acne Shooter into pores

Applying our original optical coherence tomography (OCT) technology, we obtained data indicating that Acne Shooter can infiltrate intensively into pores (Fig 6).

OCT is a technology to capture precise tomographic images of biological tissues, noninvasively (without hurting subject bodies), by applying light in the depth direction at the measurement point and obtaining information from the interference effect that occurs by the interaction of the direct and reflected light beams when they overlap and either reinforce or negate each other’s frequency. For this research, we developed a 3D-OCT skin measuring instrument exclusively for the observation of the structures of

pimples and pores. By using it in combination with our original imaging technology, we succeeded in the noninvasive, clear visualization of the internal structures of pimples and pores whose detailed observation was impossible before.

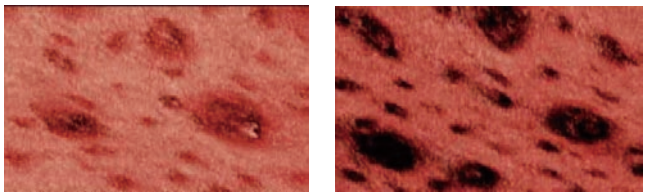

Before applying Acne Shooter　　After applying Acne Shooter

Fig. 6　Comparison of action on skin before and after application of "Acne shooter" using OCT.

4.3 Moisturizing effect of Acne Shooter

Acne Shooter infiltrating into the skin increased, by up to about seven times, the production of filaggrin, which is a protein essential for the horny layer to retain its skin protective function and moisture. The results confirmed that Acne Shooter can improve the moisture-retaining function inside the skin (Fig. 7).

Filaggrin protein exists in the horny layer of the skin and has a role in enhancing its barrier function. It also exhibits moisture retention capability when it decomposes in the horny layer into a natural moisturizing factor (amino acid).

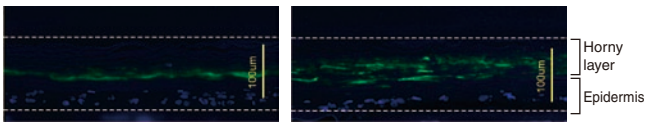

Acne Shooter not added　　Acne Shooter added

Green: Filaggrin
Blue: Nuclei

Fig. 7　Fluorescent microscopy image of 3-dimensional human dermal model.

5. Effects on skin

To verify the effects of using Lunamer AC (improvement of the pimple conditions), we performed a four-week continuous use test on thirty-six women in their 20s and 30s, in which they used, every morning and night, Lunamer AC Fiber Foam, Lunamer AC Skin Conditioner (normal/moisturizing) and Lunamer AC Gel Cream, and their before- and after-use skin conditions were checked.

Figs. 8 and 9 show the changes of the number of pimples and the amount of moisture in that four-week use test. Compared with the state before use of those products, improvements were observed in their skin conditions in regard to both the number of pimples and the amount of moisture.

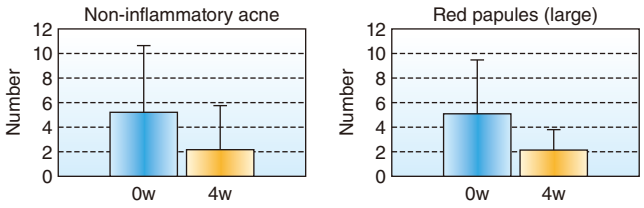

Fig. 8　Change of pimple point.

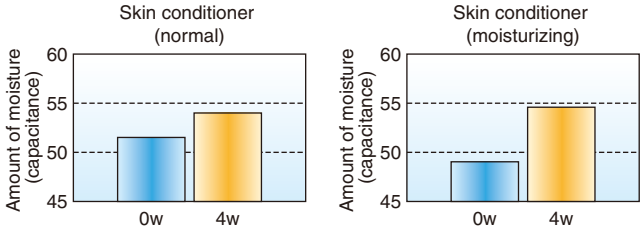

Fig. 9　Change of water content of skin.

6. Conclusion

The acne care brand, Lunamer AC, described in this paper is a range of cosmetics available only from FUJIFILM, with the aim of reducing adult pimples. They were developed using original skin analysis techniques based on image diagnosis and optical analysis technologies acquired via development activities in the digital camera and medical equipment fields and making use of our emulsification and dispersion technology derived from photography.

We will keep striving to develop science-based cosmetic technologies that only FUJIFILM can realize and to solve skin problems one by one.

Trademarks

Development of Functional Cosmetic "ASTALIFT WHITE"

Fumi KUSUDA *, Katsuhiko KANAZAWA *, Toshiyuki HONMA *,
Atsushi ORIKASA **, Gen OMURA ***, Takuji KOSUGI *, and Kozo NAGATA *

Abstract

We have developed "ASTALIFT WHITE", which contains our unique dispersion "nano-AMA", as a new skin care brand for women of all ages with skin problems such as dark spots and dullness. We focused on the brightening component "AMA", which has anti-inflammatory effects. It contains three main components, "Asiatic acid", "Madecassic acid" and "Asiaticoside". However, they are slightly soluble both in water and oil, so we developed approximately 20 nm water-dispersions, which is expected to penetrate into the skin. A comparison of "nano-AMA" with normal "AMA" showed that it had up to double the inhibitory effect on melanin production in a 3D skin model. Furthermore, "nano-AMA" greatly suppressed the dendrites' elongation of the melanocytes. We performed a clinical test for 8 weeks to evaluate the effects of the serum "ESSENSE INFILT" which is formulated with "nano-AMA". We observed a significant decrease in the melanin index, which indicates the depth of blemishes, and most subjects perceived a brightening effect.

1. Introduction

At FUJIFILM we have developed unique and functional skin care products by applying photographic expertise. On March 1, 2013, we launched onto the market a new brightening*1 skin care brand, the ASTALIFT WHITE series (nonmedicinal products), for women of all ages who have skin problems such as blemishes and dullness of the skin (Fig. 1).

Dark spots, freckles and dullness of the skin are common problems for many women in their late 20s or over. The market size of the brightening cosmetics in Japan is approximately 150 billion yen. However, according to a survey*2, nearly 70% of the users of those cosmetics are not satisfied with their effects (Fig. 2). Therefore, to respond to their needs, we have striven for the development of skin care products with high brightening effects.

Fig. 1 The new cosmetic brand "ASTALIFT WHITE".

*1 Preventing the production of melanins to suppress the outbreaks of dark spots and freckles

*2 A survey conducted by FUJIFILM

Original paper (Received December 2, 2013)

* Pharmaceutical & Healthcare Research Laboratories
Research and Development Management Headquarters
FUJIFILM Corporation
Ushijima, Kaisei-machi, Ashigarakami-gun, Kanagawa
258-8577, Japan

** Life Science Products Division
FUJIFILM Corporation
Akasaka, Minato-ku, Tokyo
107-0052, Japan

*** Analysis Technology Center
Research & Development Management Headquarters
FUJIFILM Corporation
Nakanuma, Minamiashigara, Kanagawa
250-0193, Japan

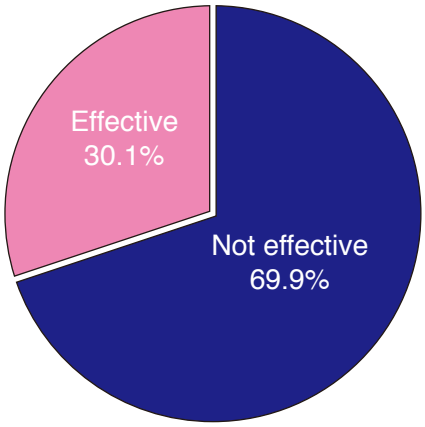

Fig. 2 Survey results on skin brightening effect of the cosmetic product.

2. Histological characteristics of dark spots

Histologically, dark spots are defined by elongated rete ridges deeply protruding into the dermis and forming buds, and a massive accumulation of melanin and an increased number of melanocytes in the basal layer of the buds.[1)] (Fig. 3) Therefore it is important to deliver brightning components to the deep skin layer in order to reduce dark spots.

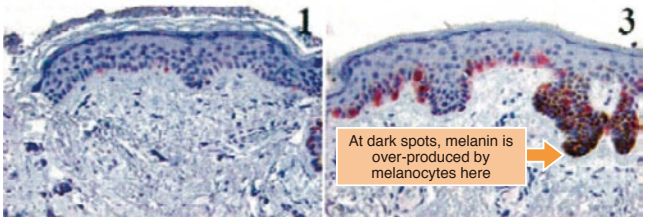

Fig. 3 Skin structure of normal region (1) and of spot (3)

3. Development of ASTALIFT WHITE

3.1 Nanoization of a brightening component, AMA, into a size of approx. 20 nm with our unique technology

Focusing on “AMA”

Centella asiatica is an Apiaceae herb that widely inhabits the subtropical zone (Fig. 4). From a legend that wild tigers cured wounds by rubbing themselves against it, the plant is also called *tiger's herb*. It is known to have excellent wound healing and anti-inflammatory effects and has thus often been used as a medicinal herb in folk remedies such as Ayurveda. Among the constituents of that Centella asiatica extract, we focused on a brightening component, AMA, which contains three ingredients with high anti-inflammatory effects: asiatic acid, madecassic acid and asiaticoside (Fig. 5).

Fig. 4 *Centella asiatica*.

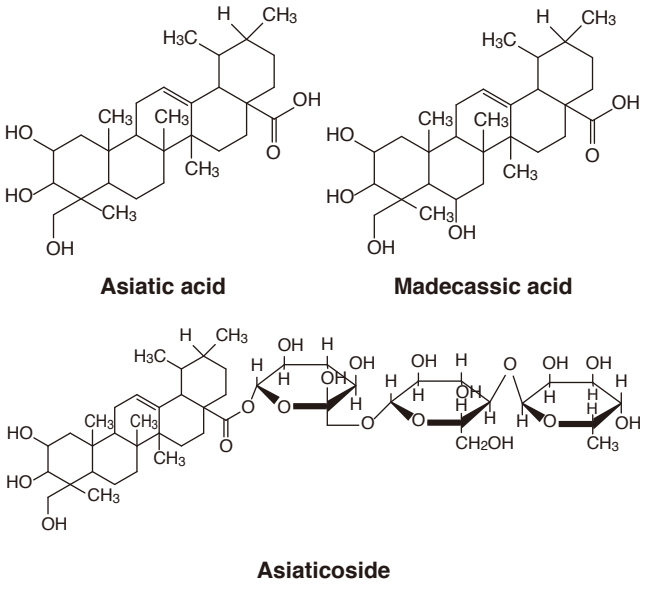

Fig. 5 The structures of Asiatic acid, Madecassic acid and Asiaticoside.

Development of "nano-AMA"

AMA, which is a brightening compound of the above three ingredients, does not easily dissolve in either water or oil. In addition, because of the similarity of their structures, the ingredients easily aggregate to each other. Therefore, in order to deliver AMA to the deep skin, it is necessary to increase its permeability by nanoizing it. To solve those problems, combining them complexly with natural amphiphilic ingredients, we established nano unit technology that effectively arranges and stabilizes those ingredients, without causing aggregation, so they can exhibit their effects. With that technology, we succeeded in the development of nano-AMA with a size of approx. 20 nm that can be expected to infiltrate into the skin (Fig. 6). With a large particle diameter, non-nanoized AMA does not let light pass through; therefore, it looks turbid. On the other hand, the nano-AMA we developed is stabilized with a very small particle diameter and looks transparent, letting light pass through (Fig. 7).

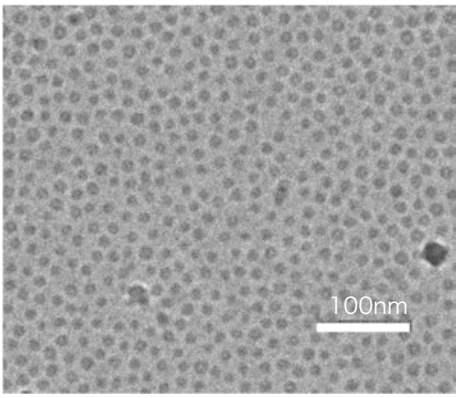

Fig. 6 Cryo-TEM image of nano-sized AMA dispersion of ice-embedded sample.

Fig. 7 "Micro-sized AMA" (left) and "nano-sized AMA dispersion" (right).

3.2 Confirmation of the effectiveness of the brightening component, AMA, with a skin equivalent

Inhibitory effect of nano-AMA on melanin production

To verify the effects of nano-AMA and non-nanoized, normal AMA on melanin-producing melanocyte cells, we conducted a test using a 3D skin equivalent containing melanocytes, with a similar structure to that of human skin (Fig. 8). The skin equivalent simulated the condition of melanocytes that exist in the deep skin.

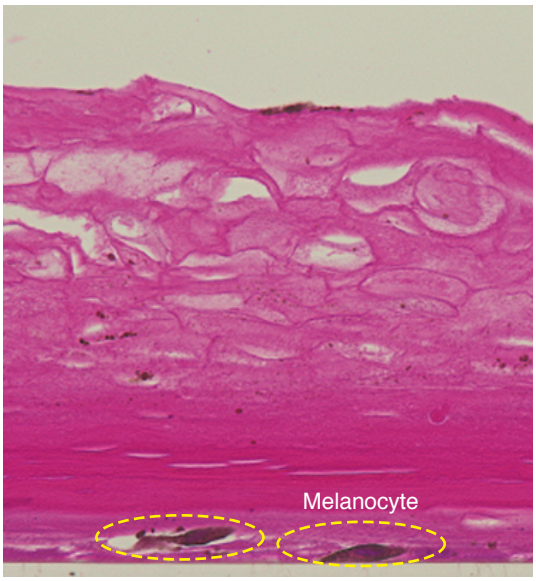

Fig. 8 3D-skin equivalent of human skin including melanocytes.

The skin equivalent was cultured for fourteen days under the following three different conditions: (i) no addition; (ii) AMA added; and (iii) nano-AMA added. Subsequently, melanins were extracted from the skin equivalent to determine the quantities. As a result, the inhibitory effect of nano-AMA on melanin production in the skin equivalent was found to be about double that of normal AMA (Fig. 9).

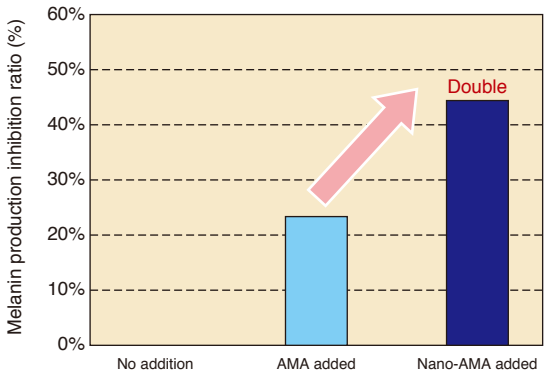

Fig. 9 Nano-sized AMA dispersion has twice the skin brightening effect of AMA.

Inhibitory effect of nano-AMA on the elongation of melanocyte dendrites

The morphological characteristics of melanocytes were also observed in the test. In the skin equivalent nano-AMA added, it was confirmed that dendrite elongation was greatly suppressed in dormancy (contraction) and thus the production of melanin was inhibited (Fig. 10). It can be considered to have happened because the permeability of AMA into the skin increased via nanoization, enhancing the effect on melanocytes.

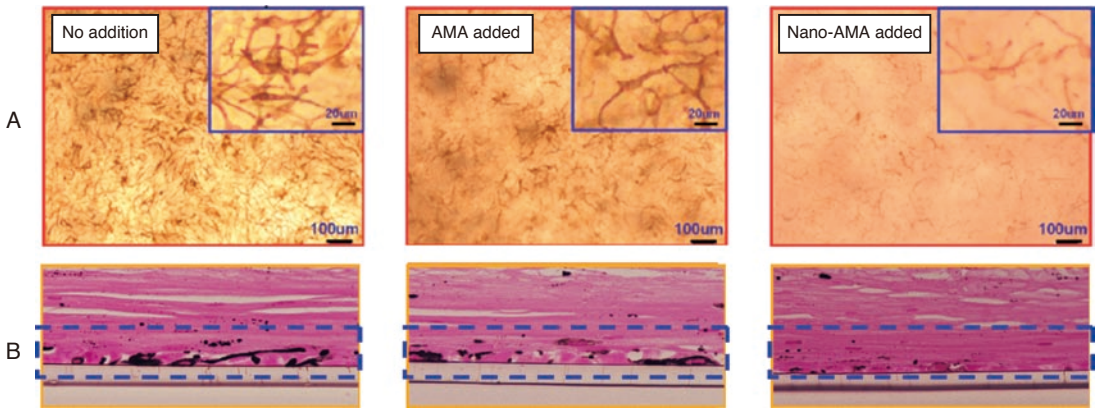

Fig. 10 (A) Nano-sized AMA dispersion suppressed dendrite elongation of melanocytes.
(B) Nano-sized AMA dispersion suppressed melanin synthesis.

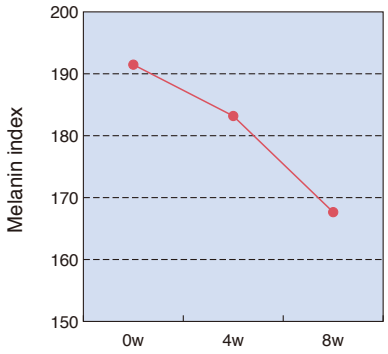

Fig. 11 Decrease of melanin index after eight weeks of continuous use.

4. Confirmation of the effects of ASTALIFT WHITE ESSENCE INFILT in vivo by a clinical test

We show the results of the clinical test to confirm the brightening effects of ASTALIFT WHITE ESSENCE INFILT which is formulated with nano-AMA below.

We recruited 26 women, aged 32-59, who had dark spots on their faces, and determined one spot to be observed for each subject. All the subjects have applied ASTALIFT WHITE ESSENCE INFILT to their entire faces twice a day for eight weeks. We measured the darkness of the spots as melanin index and took images before first application, after four weeks and eight weeks applications.

The average of melanin index of the spots was significantly decreased from 191 to 183 ($p < 0.01$) after four weeks of application, and from 183 to 168 ($p < 0.0001$) after another four weeks (Fig. 11) . As the average of melanin index of normal region was 140, those results meant the spots moved to closer normalcy by ASTALIFT WHITE ESSENCE INFILT application. Fig. 12 shows improvement of the spot as a typical case. Large spot with a well-defined border on the cheek was brightened, with indistinct border. It was obvious that the spot were brightened and not only by measured value but also by visual observation.

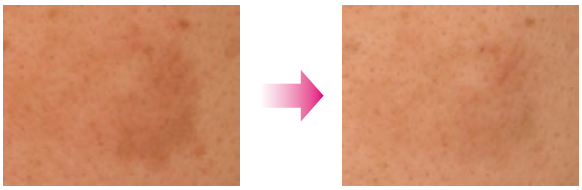

Fig. 12 A typical case of the spot improvement after four weeks application.

In addition, 77% (20/26) and 85% (22/26) subjects found their spots were improved by themselves, after four weeks and eight weeks application, respectively. Thus, we have achieved our goal of developing skin care products with high brightening effects enough to satisfy women who had not realize before.

5. Conclusion

ASTALIFT WHITE described in this paper is a functional cosmetic using original dispersions created based on the emulsification and dispersion technology we have acquired via conventional development activities in the field of photography. The effect was proved with a model close to actual human skin.

Leveraging our own expertise, we are going to keep striving for the development of functional cosmetics that create new customer value.

References

1) Lin, C. B. et al. Journal of Dermatological science. **59** (2), p.91-97 (2010)

Trademarks

- "ASTALIFT WHITE," "nano-AMA" and "ASTALIFT WHITE ESSENCE INFILT" are registered trademarks of FUJIFILM Corporation.
- Any other company names, systems and product names referred to in this paper are generally respective trade names or registered trademarks of other companies.

FUJIFILM Group's Inkjet Printhead and Technology

Yoshinori KATO*

Abstract

This paper introduces FUJIFILM Dimatix's inkjet printhead products and technologies. The broad product range includes devices with various native drop masses, print resolutions, and nozzle plate materials. Especially, stable jetting is expected with the new StarFire printhead which features a unique ink recirculation structure that maintains the ink inside the nozzle in the best condition. In addition, the world's most advanced printhead 'SAMBA' uses not only the ink recirculation but also MEMS technology, high-efficiency sputtered PZT actuator, and durable non-wet film on the nozzle plate to achieve precise and stable printing with a high resolution of 1200 dpi.

1. Introduction

FUJIFILM Dimatix, Inc. (hereinafter, "Dimatix"), whose predecessor was Spectra established in 1984, is a top manufacturer of industrial inkjet printhead products. Having bases in New Hampshire on the east coast and in California on the west coast of the United States, the company develops and manufactures wide format and material deposition inkjet printheads and high-definition printheads for commercial printing. Industrial inkjet printheads from the east-coast base are employed by many global, wide format printer manufacturers, and sign boards and outdoor advertising displays created with them can be seen all over the world. On the other hand, the high-definition printhead, SAMBA, from the west-coast base, is a product created with all the strengths of the FUJIFILM Group by integrating the inkjet technology of the east-coast base and the latest technologies of the whole Group. The product is employed in the FUJIFILM JetPress 720 digital press and has made it possible to achieve an overwhelmingly high resolution comparable to offset printers.

FUJIFILM has been developing a variety of high-performance inks mainly at its Advanced Research Laboratories in the west part of Kanagawa Prefecture in cooperation with FUJIFILM Specialty Ink Systems Ltd. and FUJIFILM Imaging Colorants Ltd. (both in the UK). In addition, via the development of printers such as the JetPress 720, the company maintains a constant effort for the enhancement of imaging technology as well as marking process technology, including the handling of Dimatix's inkjet printheads and ink drying/fixation techniques. The results are fed back to Dimatix's printhead design, which greatly contributes to the improvement of the quality of its products.

2. Outline of inkjet printheads

Table 1 presents a list of the main inkjet printhead products of Dimatix. The lineup is extensive, allowing the flexible combination of native drop volumes, resolutions and nozzle plate materials. However, when making a selection, it is necessary to take into consideration the landing accuracy of the ink, durability of the nozzle surface and ink compatibility (e.g., acid, aqueous, solvent, UV inks).

S-class and DMC printheads are suitable for material deposition such as printed electronics. The "AA" suffix of model numbers for S-class printheads indicates that they support solvent and UV inks. The SX3 and SE3 models have electrical interfaces that enable nozzle-by-nozzle drop volume control and are suitable for use requiring extremely precise ejection control (Figs. 1 and 2).

The DMC-11601 and DMC-11610 are cartridge-type printheads exclusively for the DMP2831 material printer from Dimatix (Fig. 3). Their cartridge integrates a container for liquid to be ejected with the printhead, which enables ejection and pattern drawing experiments with a mere few milliliters of liquid. Therefore, the DMC printheads are widely used throughout the world for material research in a variety of domains, not limited to use in electronics.

The Emerald (Fig. 4) is a printhead for general use including wide format printers for signs and displays. It is designed to achieve a thin exterior so the carriage of shuttle scanning is small when multiple printheads are aligned. The "AAA" suffix of the model numbers indicates that they support aqueous, solvent and UV inks.

The Polaris (Fig. 5) is a printhead with a resolution of 200 npi integrating two 100 npi printhead units aligned side by side. Dual-color types are also available with the same configuration.

Original paper (Received November 7, 2013)

* Advanced Marking Research Laboratories
Research & Development Management Headquarters
FUJIFILM Corporation
Ushijima, Kaisei-machi, Ashigarakami-gun, Kanagawa 258-8577, Japan

Table 1 Inkjet printheads of FUJIFILM Dimatix Inc.

(a) Metal nozzle plate

		Resolution			
		50npi	100npi	200npi	400npi
Native drop volume	15pl		Polaris PQ-512/15 AAA-2C	Polaris PQ-512/15 AAA	
	28pl		Galaxy 256/30 AAA		
	30pl	S-Class SE-128 AA	Emerald QE-256/30 AAA Galaxy 256/30 HM		StarFire SG1024/M-A StarFire SG1024/M-C
	35pl		Polaris PQ-512/35 AAA-2C	Polaris PQ-512/35 AAA	
	50pl	S-Class SM-128 AA	Galaxy 256/50 AAA		
	80pl	S-Class SL-128 AA	Emerald QE-256/80 AAA Galaxy 256/80 AAA Galaxy 256/80 HM Polaris PQ-512/85 AAA-2C	Polaris PQ-512/85 AAA	

(b) Silicon nozzle plate

		Resolution		
		50npi	100npi	1200npi
Native drop volume	1pl		DMC-11601	
	2pl			Samba 1200
	8pl	S-Class SX3		
	10pl		DMC-11610 Sapphire QS-256/10 AAA	
	30pl		Sapphire QS-256/30 AAA	
	35pl	S-Class SE3		
	80pl		Sapphire QS-256/80 AAA	

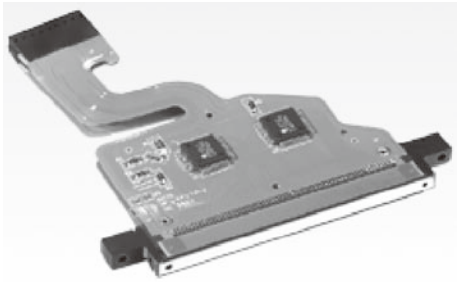

Fig. 1 S-Class SE128 AA

(a) DMP2831 (b) DMC printhead

Fig. 3 Material printer DMP2831 and DMC printhead

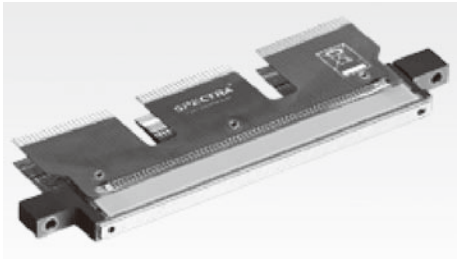

Fig. 2 S-Class SE3

Fig. 4 Emerald printhead

Models with numbers suffixed in “2C” can contain two kinds of inks.

The Sapphire is a type using a silicon nozzle plate. With the high-precision processed nozzle, it achieves a very fine droplet volume of 10 pL at the minimum and has a high landing accuracy ejection.

The StarFire printhead (Fig. 6), just like the SAMBA printhead described later, has a mechanism allowing the collection of

ink that has even reached the vicinity of the nozzle. By injecting new ink into the printhead, with an externally installed circulation system to collect unused ink inside, it is possible to maintain the ink inside the nozzle in an always fresh and optimal condition.

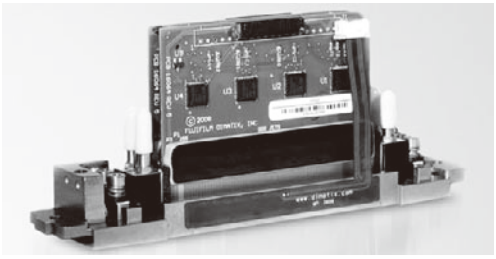

Fig. 5 Polaris printhead

That ensures stable jetting without causing any adherence of ink around the nozzle even if the ink itself is prone to becoming dry or the printhead is in a high-temperature and dry environment. In addition, the nozzle plate is replaceable; therefore, in the case of nozzle clogging, there is no need to replace the whole printhead. Two types are available in the series: SG1024/M-A for aqueous ink and SG1024/M-C for ceramic ink.

The Galaxy 256/30HM and Galaxy 256/80HM are hot-melt ink printheads. They heat solid ink, which is like clay at room temperature, with a built-in device up to 125°C and eject liquefied ink (Fig. 7).

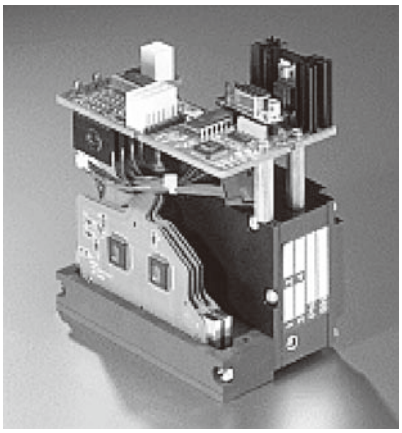

Fig. 7 Galaxy 256/30 HM

Fig. 6 StarFire printhead

3. High-definition inkjet printhead, SAMBA

Fig. 8 shows the exterior of the SAMBA printhead. The base shape is a parallelogram; therefore, a wider line head can be created via in-line connection. Because the line head width is narrower than that of the heads connected in a staggered array, it is possible to reduce the equipment size by arranging multiple line heads next to each other and to suppress color drift due to the oblique motion of media. Moreover, the marking conditions are uniform over the whole line head area, which greatly mitigates the precision level required for the positioning of neighboring heads.

The following are the technological advantages of the SAMBA printhead.

(1) Manufacturing process with MEMS technology

The silicon-base ink channel in the vicinity of the nozzle is manufactured via the microelectromechanical (MEM) process based on semiconductor lithography technology. The wafers are connected to each other by the interatomic force of the silicon interface and there are very few cases in the world in which such connection is realized on a commercial basis. The precision of

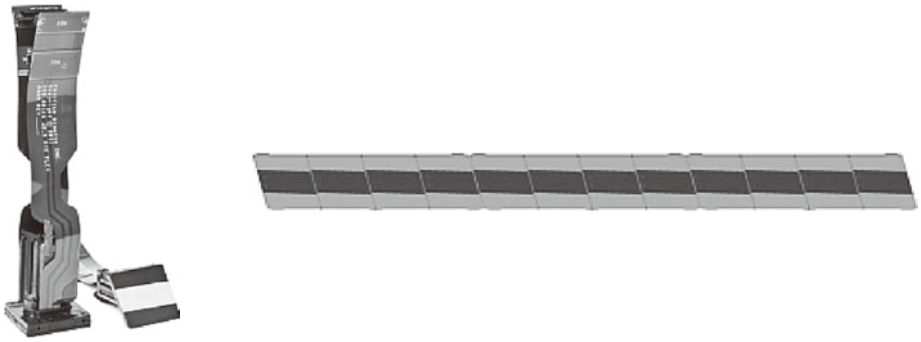

(a) Figure (b) Inline stitching

Fig. 8 SAMBA printhead

the processing is very high, which prevents the occurrence of variation between individuals in their fluid path properties and, as shown in Fig. 9, contributes to the achievement of extremely small deviation in the jet direction.

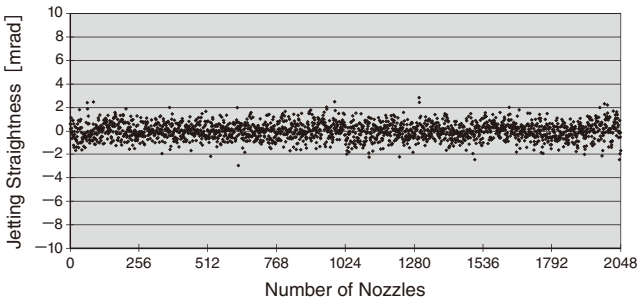

Fig. 9 Example of the jet straightness characteristics

(2) Sputtered PZT

The PZT actuator of the SAMBA printhead is created based on our original sputtered PZT (or lead zirconate titanate) film deposition technology that achieves an extremely high piezoelectric constant. Conventionally, a method has been used in which bulk PZT is thinned via polishing. However, with our sputtering technology, it has become possible to streamline production processes and stabilize the ejection performance. In addition, sputtered PZT films are highly heat-resistant, which improves flexibility in high-temperature processes and enables the stable formation of protective films with low moisture permeability on the surface. That prevents moisture penetration from affecting the life of the product. A rigorous endurance test, in which high-voltage pulses were applied 700 billion times in a high-humidity environment, achieved an excellent result that none of the 2,048 PZT actuators failed at all.

(3) Structure that enables ink circulation

The SAMBA printhead has the same mechanism as the previously described StarFire printhead that collects ink that has already reached the vicinity of the nozzle.

(4) Non-wet coating

In the SAMBA printhead, an inorganic film is deposited as a base over the silicon nozzle plate surface, on which organic materials containing fluorine are densely arranged. In that way, a homogeneous, highly liquid-repellent film is formed and improves tail break off liquid when it is ejected, achieving stable jets of fine droplets. The coating is so thin that it does not affect the shape of the nozzle and will not be the cause of deviation in the jet direction. In addition, with its high adhesion to the base material (silicon), the film cannot easily be scratched off even if the nozzle surface is wiped by a rubber blade, etc. The film keeps high liquid repellence for a long time and has a low risk of clogging the nozzle with its shavings in the downstream of wiping. The nozzles can thus maintain stable ejection for over a long period of time.

(5) Nozzle arrangement

A total number of 2,048 nozzles are arranged in a 32-by-64 matrix. Their relative positions are optimally designed to avoid coalescence in which surface tension combines ink droplets ejected onto a medium. The resolution in the direction of the printhead width is fixed at 1,200 dpi and that in the media feeding direction is 1,200 dpi or 600 dpi. In high-resolution mode of 1,200 × 1,200 dpi, images are made of a straight grid of dots while, in high-speed mode of 1,200 × 600 dpi, images are made of a gird of dots slanted by 45° (staggered arrangement) (Fig. 10). In that way, higher-definition images can be realized with the same productivity as the resolution of 600 × 600 dpi.

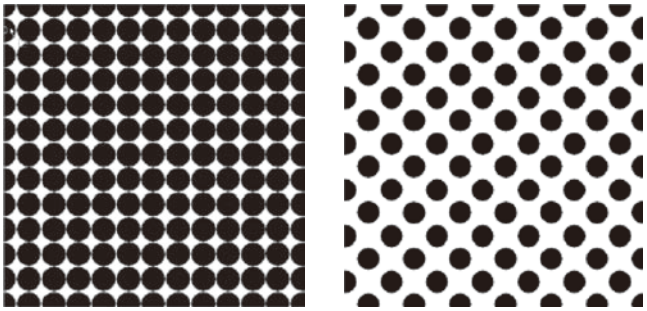

Fig. 10 Image structure

(6) Internal protective film

All the channels formed in the silicon inside the printhead are covered with protective films. That allows the use of an extensive range of inks. Moreover, should foreign substances adhere to the walls of those channels during the printhead production process, the covering protective film does not let them easily come off and thus prevents their inclusion in ink.

The SAMBA printhead has the following three advantages that may allow its application to the field of printed electronics.

1) Small native drop volume
   The drop volume of the printhead commercialized for the JetPress 720 digital printer is 2 pL at the minimum. Technologically, even a volume of 1 pL or smaller is possible to design.
2) High accuracy of drop landing positions
   This is advantageous when it is required to eject ink onto a substrate with high accuracy.
3) Little contamination to liquid fillings
   The channels inside the printhead are made via etching, allowing little adhesion of foreign substances. The internal protective film also contributes to the prevention of the contamination of ink.

Dimatix provides development kits for the evaluation of the flight conditions of the ink drops and the quality of print with the SAMBA printhead. With them, a printhead evaluation environment can be established in a short period.

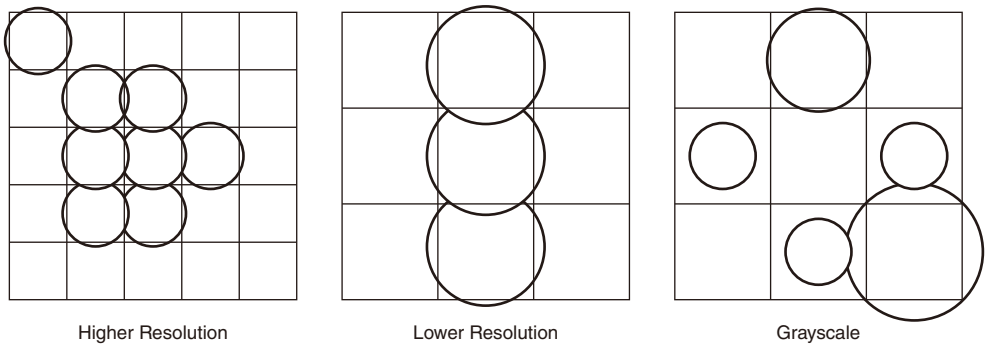

Fig. 11 Imaging by Versa Drop technology

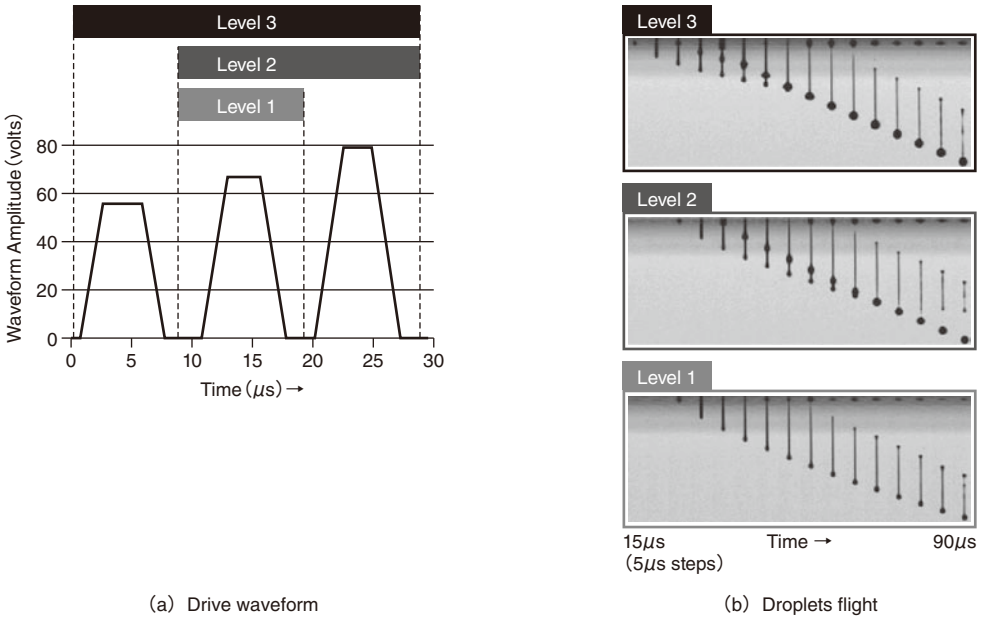

(a) Drive waveform (b) Droplets flight

Fig. 12 Example of driving by Versa Drop

4. Multi-drop technology

Dimatix employs Versa Drop technology that controls droplet volumes by applying multiple pulses continuously to PZT actuators. That enables the flexible adjustment of droplet volumes ejected by printheads, for example, between 25 and 65 pL for the SG1024/M-A and even in a wide range between 80 and 200 pL for the Emerald QE-256/80 AAA. A single printhead can thus generate high-resolution as well as voluminous images.

In addition, individually setting those multiple pulses to on or off for each nozzle enables the production of gray-scale images. That makes it possible not only to realize low graininess and high-density printing at the same time but also to adjust nozzles in a bad ink drop condition via image processing (Fig. 11).

Fig. 12 shows an example of Versa Drop drive waveforms. With that technology, three ejection stages from Level 1 to Level 3 are available; however, because the droplet volume created by a single pulse at a time does not vary significantly, it is possible to maintain the meniscus of nozzles in an optimal condition. Thus, long-term stable ejection is ensured.

5. Conclusion

As described above, it is believed that Dimatix's inkjet printhead products and the employed technologies are all excellent. However, to realize high-quality patterning and printing, it is essential to make a high-level combination of inks, printhead handling techniques and marking process technologies. The FUJIFILM Group is going to continue enhancing its technology in the development of its own brand printers and in cooperation with other global printer vendors and to contribute to the advancement of science, technology and industry.

Trademarks

Preparation of Nb-doped PZT Thin Film with High Piezoelectric Performance and Its Application to MEMS Devices

Takamichi FUJII*, Takayuki NAONO*, Akihiro MUKAIYAMA*, Takami ARAKAWA*,
Yoshikazu HISHINUMA**, Youming LI**, and Jeffrey BIRKMEYER**

Abstract

We have developed a method of forming PZT films on silicon substrates with a high piezoelectric coefficient using RF sputtering. Films have been formed on 6-inch wafers with thickness variation of less than +/− 5% across the entire wafer. Our PZT film has an unusually high content of Nb dopant (13%) which results in 1.7-fold higher piezoelectric coefficient than sputtered PZT films previously reported. The X-ray diffraction patterns of our PZT film formed on a 6-inch wafer demonstrate that the film is in a perovskite phase with (100) orientation which partly accounts for its high piezoelectric performance. One of the unique properties of our sputtered PZT film can be observed in the P-E hysteresis loop shifted to the positive electric field, suggesting that the polarization axes have been aligned in a certain direction beforehand, making a post-deposition polarization process unnecessary. We applied the PZT film to an ink-jet head and micro-mirror as a MEMS device application, and demonstrated high actuation performances of both devices.

1. Introduction

The actuators of ink-jet heads, etc., use piezoelectric materials for their driving units. To achieve higher definition and higher performance from those devices, it is necessary to refine the actuator mechanisms by applying semiconductor technologies such as microelectromechanical systems (MEMS). To that end, research and development have been undertaken that enable piezoelectric materials to be changed from conventional bulk materials that require polishing to thin films.[1)]

Normally, long-established PZT materials are used for that purpose. The piezoelectric performance (d_{31}) of undoped genuine bulk PZT materials is −93 pm/V and that is not sufficient for actuators. Therefore, in general, third component-added denatured PZT or materials in the relaxor system are used. Among the methods to make piezoelectric materials into thin films are the sol-gel process, sputtering, aerosol deposition and chemical vapor deposition.[2)-9)] To form good-quality films with a high piezoelectric constant, those methods have introduced an annealing step after film deposition or techniques utilizing epitaxial growth with single-crystal substrates to enhance crystallization. Currently, however, films formed on silicon substrates compatible with the MEMS process have not been able to achieve sufficiently high piezoelectric performance.

Therefore, by using sputtering, which is highly versatile and enables easy film formation in the order of micrometers, we formed a PNZT film with a piezoelectric constant enhanced by doping PZT with Nb on a silicon substrate via electrodes. This paper describes the characteristics of that film and its application to MEMS devices.

2. Nb-doped PZT thin film by sputtering[10)-12)]

2.1 Nb-doped PZT thin film

PZT is a complex oxide having a perovskite structure, expressed by the chemical formula $Pb(Zr_xTi_{1-x})O_3$. Fig. 1 illustrates the structure. Pb^{2+} ions are positioned at A sites, and Zr^{4+} or Ti^{4+} ions occupy B sites. At a temperature not greater than the Curie point, B-site ions, Zr^{4+} or Ti^{4+}, shift from the center of the crystal and that causes spontaneous polarization. Those ions undergo a displacement in response to the external electric field, which appear as ferroelectricity and piezoelectricity. In this development, a trial was made to increase the piezoelectric constant with a material created by doping the B sites with Nb (hereinafter, "PNZT").

Original paper (Received December 20, 2013)

* Advanced Marking Research Laboratories
Research & Development Management Headquarters
FUJIFILM Corporation
577 Ushijima, Kaisei-machi, Ashigarkami-gun, Kanagawa
258-8577 Japan

** FUJIFILM Dimatix, Inc.
2230 Martin Avenue, Santa Clara, CA 95050, U.S.A.

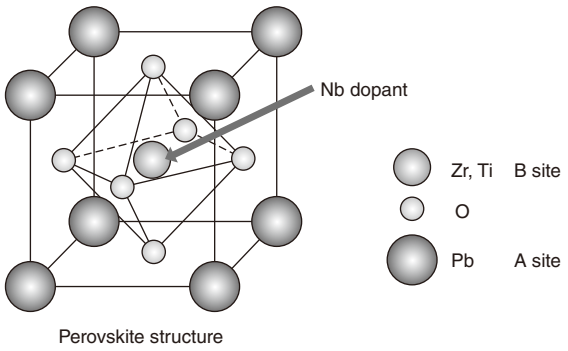

Fig. 1 Crystal structure of PZT.

2.2 Conditions for the forming of a sputtered PNZT thin film and its evaluation method

Using a silicon substrate with a (100) orientation, we formed, as follows, a PNZT thin film with our original RF magnetron sputtering equipment that allows 6-inch film formation. First, a 20-nm Ti adhesion layer was formed on the silicon substrate by sputtering. Then, a 150-nm lower Ir electrode was deposited. On that substrate, a PNZT film was formed by sputtering using the $Pb_{1.1}(Zr_{0.46}Ti_{0.42}Nb_{0.12})O_3$ target. The ratio of Zr to Ti in the target was set to 52:48, which is the same as that of the morphotropic phase boundary (MPB). That composition achieves the highest piezoelectric constant and electromechanical coupling coefficient; therefore, it is suitable for actuators. Also, to further improve its piezoelectric properties, we made a 12% doping of the target with Nb (perovskite B-site conversion). Under those conditions and at a deposition temperature between 450 and 550°C, we succeeded in the formation of a stable PNZT film with a perovskite structure.

For the evaluation of the formed PNZT film, we checked its crystal structure and orientation with X-ray diffraction (XRD), observed the cross-sectional structure with a scanning electron microscope (SEM) and a transmission electron microscope (TEM), and performed composition analysis with X-ray fluorescence (XRF). To evaluate its ferroelectric properties, the P-E hysteresis loop was measured and, using an impedance analyzer, the dielectric constant and loss tangent values were measured. In addition, we created a diaphragm structure via micromachining and evaluated the film's mechanical displacement properties by applying a voltage and measuring the magnitude of the resulting displacement with a laser Doppler vibrometer. The piezoelectric constant (d_{31}) was determined via simulation and the value was evaluated with the $e_{31, f}$ measuring equipment (manufactured by aixACCT). For some evaluation items, comparison was made with genuine PZT samples without Nb doping.

2.3 Structure and composition

Fig. 2 shows the results for the XRD measurement of the PNZT film formed on the 6-inch wafer. The measurement positions are at the center of the wafer and at locations 5 cm above, below, to the left and to the right of the center. The observation of the diffraction peaks revealed that the film did not have any peaks other than the perovskite phase. Therefore, it can be said that PNZT with a single-phase perovskite structure was created. With regard to the crystal orientation, only a peak attributable to the (100) orientation appeared, which means the crystal was perfectly oriented in that direction.

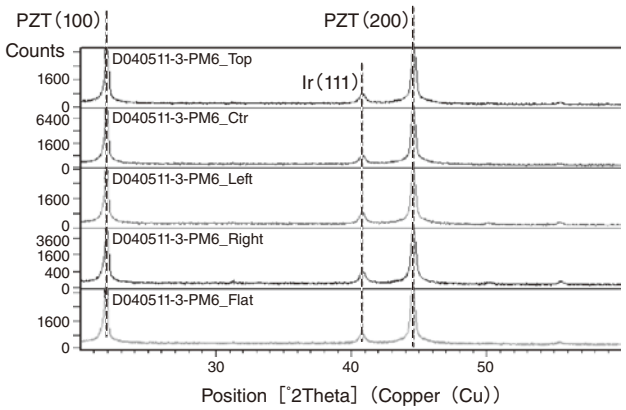

Fig. 2 X-Ray diffraction pattern of PNZT film.

The in-plane composition distribution of the film was also measured with XRF. The results obtained are shown in Table 1, according to which, a PZT film containing approximately 13% Nb was formed evenly on the wafer. While doping general bulk materials with Nb at a concentration of 3% or more may cause separation, form a pyrochlore phase or decrease performance, this film incorporates Nb atoms in without such problems. Under the deposition conditions of this film, doping with an even larger amount of Nb caused cracks on the film. Thus, no higher level of Nb doping was used.

Fig. 3 presents the cross-sectional SEM and TEM images of the obtained film. The film having a columnar structure is densely packed without gaps between grain boundary or at the electrode

Table 1 Composition of 6-inch sputtered PNZT film at 5 locations on a wafer.

Position	Pb/(Zr + Ti + Nb)	Zr/(Zr + Ti)	Ti/(Zr + Ti)	Nb/(Zr + Ti + Nb)
Top	1.096	0.505	0.495	0.130
Left	1.099	0.505	0.495	0.130
Center	1.121	0.506	0.494	0.128
Right	1.085	0.503	0.497	0.130
Flat	1.086	0.502	0.498	0.129

interface. A fine PNZT film was formed from the lower electrode interface.

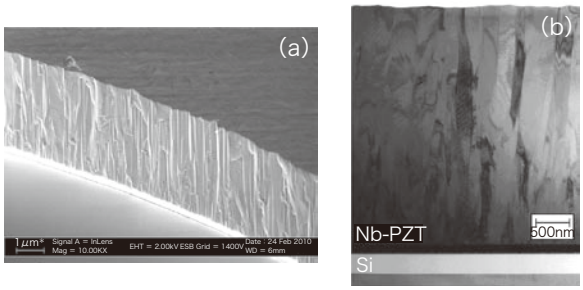

Fig. 3 SEM and TEM images of PNZT cross-sections: (a) SEM image and (b) TEM image.

2.4 Piezoelectric and electrical properties

We formed an upper electrode on the obtained film and measured the P-E hysteresis to evaluate its ferroelectric properties. The results obtained are shown in Fig. 4. For comparison, the data for genuine PZT are also shown. According to the figure, the PNZT film achieved an excellent hysteresis loop, which is significantly shifted to the right, compared with genuine PZT. That means, as one of its major characteristics, the film has a polarized state right from its creation (described later).

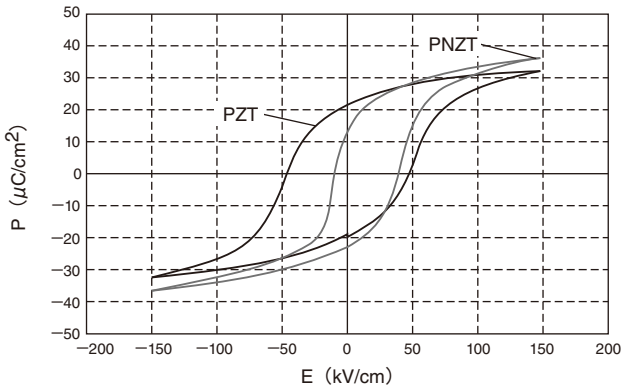

Fig. 4 P-E hysteresis loops of PZT and PNZT.

Table 2 contains the thickness, dielectric constant (ε), loss tangent (tan δ) and maximum value of remanent polarization (P_{rmax}) of the film on the 6-inch wafer. Each property was relatively uniform across the wafer.

Table 2 Film thickness, dielectric constant, tan δ and max. polarization of PNZT film at 5 locations on a wafer.

Position	Thickness (μm)	ε	tan δ	P_{rmax} (μC/cm²)
Top	3.01	1161	0.020	38.8
Left	2.96	1139	0.020	38.9
Center	3.14	1209	0.022	37.6
Right	2.99	1136	0.020	39.4
Flat	3.09	1184	0.020	38.9

2.5 Piezoelectric constant evaluation, drive properties and other properties of the PNZT thin film

To calculate the piezoelectric constant, we created a diaphragm structure as shown in Fig. 5 with MEMS technology and, while applying voltage between the upper and lower electrodes, measured the displacement magnitude at the center of the diaphragm with a laser Doppler vibrometer. Subsequently, the piezoelectric constant, d_{31}, was determined with the finite element method.[10), 11)] For the Young's modulus of the PNZT film, which is an important parameter required for that determination, we used 49GPa calculated from the resonance frequency of the structure. As a result, $d_{31} = -259$ pm/v was obtained for this PNZT film. The value was approximately 1.7 times that of conventional material.

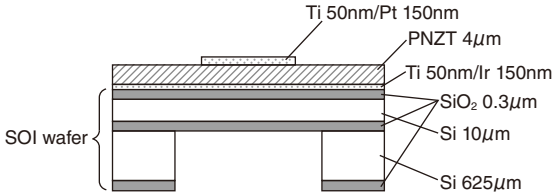

Fig. 5 Schematic of diaphragm structure for displacement measurement.

Separately, we measured the $e_{31,f}$ piezoelectric constant with the four-point bending system aix4PB manufactured by aixACCT Systems. That piezoelectric constant can be evaluated by reading the electrical charges that are generated in the piezoelectric film via the positive piezoelectric effect caused by the application of stress with the four-point bending method to the laminated cantilever of a silicon substrate (25 mm^L × 3 mm^W), lower electrode, piezoelectric film and upper electrode. As shown in Fig. 6, $e_{31,f} = -25.1$ C/m² was obtained for this PNZT film, which is the highest performance for mass-production products currently available.

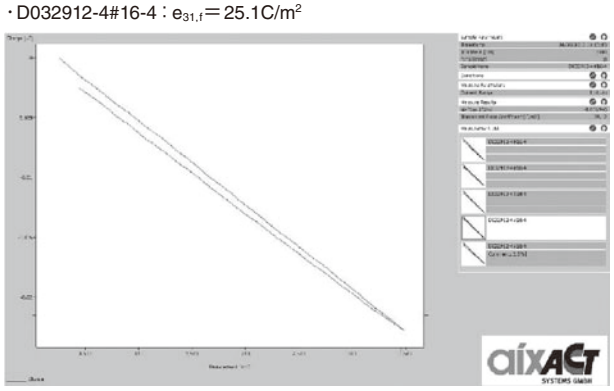

Fig. 6 Piezoelectric coefficient $e_{31,f}$ of PNZT film.

With a diaphragm structure as shown in Fig. 5, we also evaluated the drive properties of the film by applying voltage to the upper electrode and connecting the lower electrode to ground potential. The results obtained are presented in Fig. 7. When negative voltage was applied to the upper electrode of the obtained device, the displacement increased linearly (①) and, as the voltage was reduced, it decreased linearly (②). Next, when positive voltage was applied, the polarity of the piezoelectric material was inverted near its coercive electric field (at approximately 10 V), chang-

ing the direction of displacement, and the displacement became greater with the voltage. Then, as the voltage was reduced, the displacement occurred in the way shown as ④. Although this is not given in Fig. 7, when negative voltage was applied again, the displacement exhibited the same tendency again as shown at ①. Thus, the obtained PNZT film has the characteristic of returning to the previous state immediately even if the polarity is inverted. That is, the PNZT film is a strong spontaneously polarized film, initially in the direction that will achieve excellent displacement with negative drive; therefore, even if it is polarized in the opposite direction, the film is restored to the previous state immediately. Incidentally, because of the dependence of its capacitance on temperature, the Curie point of the film was the same level as general PZT materials (approximately 340°C). Moreover, it was revealed that the PNZT film spontaneously keeps its polarity in the same direction and even if it is heated, it re-polarizes itself.

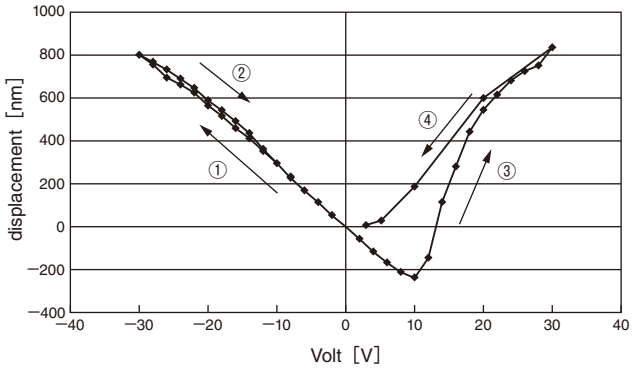

Fig. 7 Displacement of PNZT film.

In summary, the obtained film has the following characteristics: it is pre-polarized immediately after its formation; it is not easily polarized in the direction opposite to its spontaneous polarization; and it restores its polarity even if it is heated. Those characteristics can be considered to be advantageous for the application of the film to devices, indicating that no depolarization occurs even in high-temperature processes such as reflow and no post-deposition polarization process is necessary, and thus they can achieve long-term stable drive performance.

Fig. 8 indicates the I-V properties measured to investigate the breakdown voltage of a 3-μm-thick PNZT film. According to the figure, the breakdown voltage was not smaller than 300 V. The reason for negative voltage being applied was that, as previously described, it was the pre-polarization and actual drive direction of the film: that is, negative voltage was applied to the upper electrode when the lower electrode was connected to ground potential. It can be considered that such a high breakdown voltage is achieved because the film is dense and contains no gaps as shown in Fig. 3. Applying this high breakdown-voltage PNZT film to devices enables drive design with sufficient capacity.

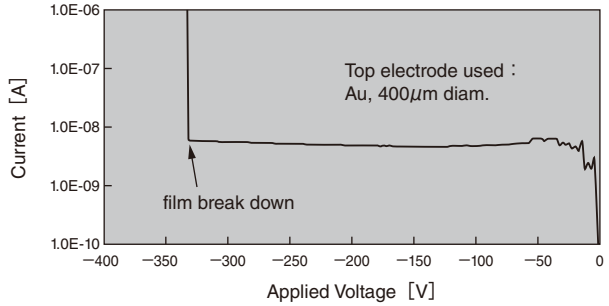

Fig. 8 *I-V* measurement on 3μm-thick PNZT film.

However, because breakdown voltage can be affected by damage via the MEMS formation process, it is necessary to handle the film with care in the process of its application to devices.

3. Application examples

3.1 Application to ink-jet heads

We applied the PNZT film we developed in this research to ink-jet heads. Fig. 9 illustrates the outline drawing of an ink-jet head using a piezoelectric material. Conventional ones are made by polishing a bulk material attached to a silicon substrate. On the other hand, a PNZT film is directly formed via sputtering, which reduces variations in thickness and differences in levels as well as improves homogeneity (Fig. 10). Bulk materials are difficult to handle

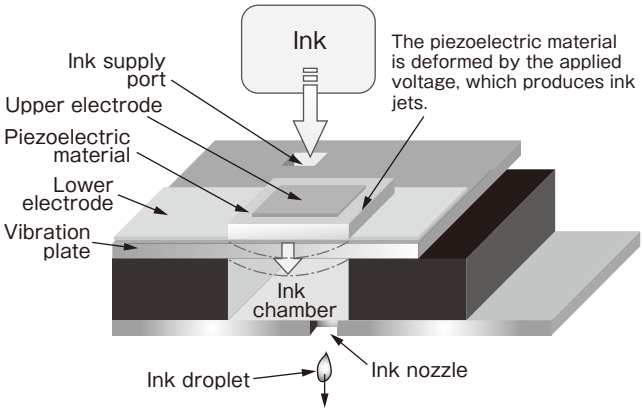

Fig. 9 Image of ink jet head.

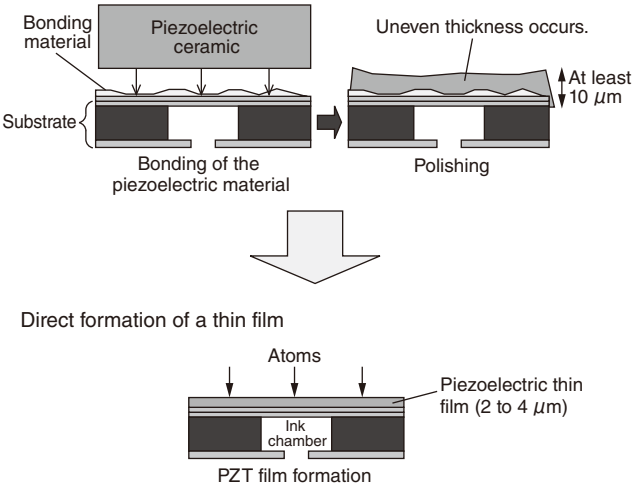

Fig. 10 Process of fabricating ink jet heads using bulk PZT and thin-film PZT.

because they can be depolarized and thus their polarization quality degrades considerably after reflow. However, as already described, this PNZT film does not need a post-deposition polarization process and does not change with heat; therefore, it is highly durable and can provide a technological margin for process conditions.

Fig. 11 presents a photo of a head module manufactured by FUJIFILM Dimatix using this PNZT film. Having incorporated MEMS technology, the ink-jet head realized a resolution of 1,200 dpi, droplet volume of 2 pL, 2,048 nozzles/inch, frequency of 100 kHz and high durability. Thus, it has an extensive range of uses.

Fig. 11 MEMS ink jet head“SAMBA”.

3.2 Application to micromirrors

Drive methods for micro scanners are divided into the following four categories: electrostatic; electromagnetic; thermoelectric; and piezoelectric. Each method has its own advantages but the piezoelectric method seems particularly promising because it can be applied to a variety of uses, achieving a large driving force, in spite of its compact size and relatively low voltage requirements.[13] As part of medical applications, FUJIFILM has already developed micromirrors for incorporation into endoscopes.[14] Fig. 12 shows a conceptual image of the obtained device and a photo of the MEMS mirror. Being held with meandering hinges associated with the cantilever structures driven at both ends, the mirror rotates as the cantilevers move up and down. The drive properties of the device can be changed by altering the thickness, width and number of turning paths of the hinges.

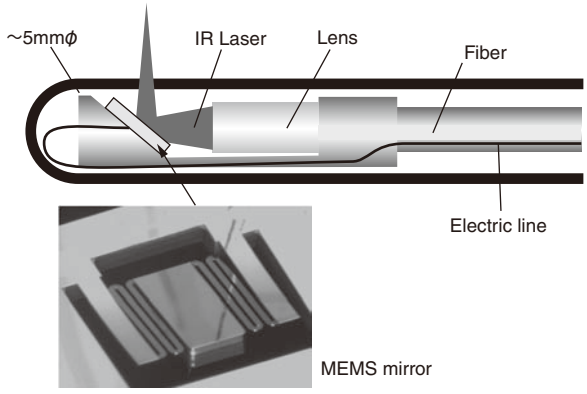

Fig. 12 Typical OCT probe with MEMS scanner.

Fig. 13 indicates the drive properties of the above described device when it uses a PNZT film and a genuine PZT material, each with and without polarization. According to the figure, the device using genuine PZT achieved an optical scan angle of approximately 19° without polarization (as-deposition state) at a drive voltage of 0.5 V. With polarization, the angle greatly increased and an optical scan angle of approximately 43° was achieved at the same drive voltage. That means, the genuine PZT film requires polarization. On the other hand, the one using a PNZT film achieved an optical scan angle of approximately 128° at the same drive voltage, regardless of polarization.

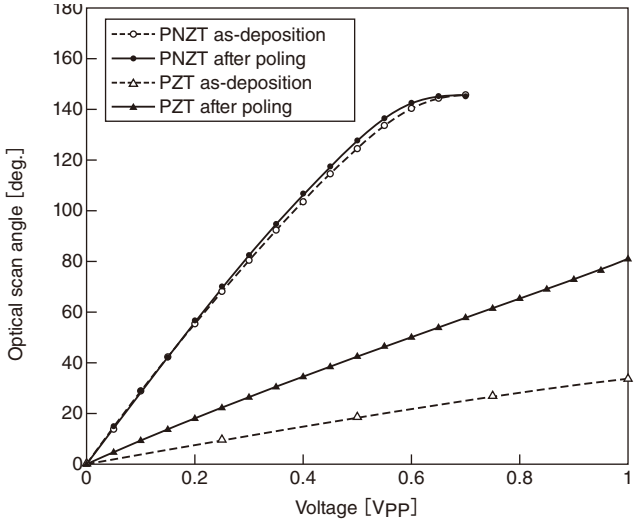

Fig. 13 Voltage response of the micro mirror driven by PNZT and PZT thin films.

The results confirmed that the PNZT film we developed has a larger piezoelectric constant than conventional genuine PZT materials and does not require polarization.

As regards MEMS mirrors, we created some other structures with different resonance frequencies and evaluated their drive frequencies and optical scan angles. To compare the performance with conventional methods including piezoelectric, electromag-

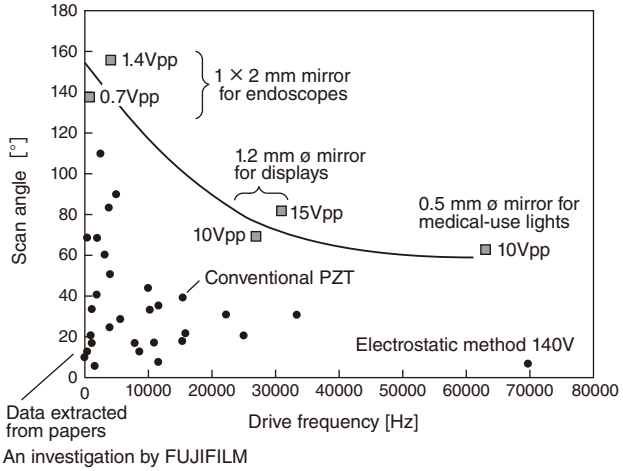

Fig. 14 Comparison of micro mirror performance based on the literature.

netic and electrostatic techniques, data cited from other papers are plotted together in Fig. 14.[15)-22)] In general, the higher the drive frequency, the smaller the scan angle of the mirror becomes. Therefore, as a whole, the higher the drive frequency, the smaller the scan angle becomes. For this research, we developed three types of mirrors: the above described low-speed mirror for endoscopes (resonance frequency of approximately 100 Hz); a middle-speed mirror for displays (approximately 25 kHz); and a high-speed mirror intended for medical, fast wavelength-swept devices (approximately 65 kHz). Each mirror achieved a larger scan angle than the values reported for conventional ones. We believe that it happened because the performance of the PNZT piezoelectric material used as their drive source is superior to conventional ones.

The overall results confirmed that, by using our PNZT film in combination with MEMS technology, it is possible to create higher-performance MEMS mirrors than ever. We are planning to develop products with higher added value by further improving the performance of the piezoelectric film and designing devices that make the most of its characteristics.

4. Conclusion

We formed an Nb-doped PZT film (PNZT film) on a 6-inch wafer via sputtering and evaluated its properties. The PNZT film thus obtained achieved piezoelectric constants, d_{31} and $e_{31,f}$, of −250 pm/V and −25.1 C/m^2 respectively, which proves that the performance of the film is much higher than conventional genuine PZT materials. Across the 6-inch plane, the film exhibited excellent structure and homogeneity in its film thickness and composition. In addition, it was confirmed that the film requires no polarization process because it is pre-polarized immediately after its deposition.

We created an ink-jet head with that PNZT film, realizing high resolution, high-speed printing and high reliability. Moreover, in its application to MEMS micromirrors, having achieved larger scan angles than conventional products, we are convinced that it can be developed for use with various-purpose mirrors.

The PNZT film we developed has unconventionally excellent properties. We will seek to advance that technology into various useful devices, while combining MEMS technology compatible with it and will thereby present new values in society.

References

1) Muralt, P. J. Micromech. Microeng. **10** (2), p.136 (2000)
2) Wolf, R. A.; Trolier-McKinstry, S. J. Appl. Phys. **95** (3), p.1397-1406 (2004)
3) Ledermann, N.; Muralt, P.; Baborowski, J.; Forester, M.; Pellaux, J. P. J. Micromech. Microeng. **14** (12), p.1650 (2004)
4) Sakashita, Y.; Ono, T.; Segawa, H.; Tominaga, K.; Okada, M. J. Appl. Phys. **69** (12), p.8352-8357 (1991)
5) Shimizu, M.; Fujisawa, H.; Shiozaki, T. J. Cryst. Growth. **174**, p.464-472 (1997)
6) Takayama, R.; Tomita, Y. J. Appl. Phys. **65** (4), p.1666-1670 (1989)
7) Kanno, I.; Kotera, H.; Wasa, K.; Matsunaga, T.; Kamada, T.; Takayama, R. J. Appl. Phys. **93** (7), p.4091-4096 (2003)
8) Lebedev, M.; Akedo, J. Jpn. J. Appl. Phys. **41**, p.6669-6673 (2002)
9) Shepard, J. F. Jr.; Chu, F.; Kanno, I.; Trolier-McKinstry, S. J. Appl. Phys. **85** (9), p.6711-6716 (1999)
10) Fujii, T.; Hishinuma, Y.; Mita, T.; Arakawa, T. Solid State Commun. **149** (41), p.1799-1802 (2009)
11) Fujii, T.; Hishinuma, Y.; Mita, T.; Nakano, T. Sens. Actuators A. **163** (1), p.220-225 (2010)
12) Hishinuma, Y.; Li, Y.; Birkmeyer, J.; Fujii, T.; Nakano, T.; Arakawa, T. Nanotechnology 2012 Electronics, Devices, Fabrication, MEMS, Fluidics and Computation: Technical Proceedings of the 2012 NSTI Nanotechnology Conference and Expo Volume 2. Santa Clara, 2012-06-18/21. NTIS, CRC Press, 2012, 878p., 978-1-4665-6275-2.
13) Wolter, Alexander; Hsu, Shu-Ting; Schenk, Harald; Lakner, Hubert. Proc. SPIE. **5719**, MOEMS and Miniaturized Systems V, p.64-75 (2005)
14) Naono, T.; Fujii, T.; Esashi, M.; Tanaka, S. J. Micromech. Microeng. (In press).
15) Smits, J. G.; Fujimoto, K.; Kleptsyn, V. F. J. Micromech. Microeng. **15** (16), p.1285 (2005)
16) Ohtsuka, Y.; Nishikawa, H.; Koumura, T.; Akita, S.; Hattori, T. Denkigakkai Ronbunshi E (IEEJ Transaction on Sensors and micromachines). **116** (8), p. 345-352 (1996)
17) Tsaur, J.; Zhang, L.; Maeda, R.; Matsumoto, S.; Khumpuang, S. Jpn. J. Appl. Phys. **41**, p.4321-4326 (2002)
18) Nippon Signal Co., Ltd. http://www.signal.co.jp/vbc/mems/ecoscan/, (reference, 2014-02-12).
19) Asai, N.; Matsuda, R.; Watanabe, M.; Takayama, H.; Yamada, S.; Mase, M.; Shikida, M.; Sato, K.; Lebedev, M.; Akedo, J. Proceedings of the IEEE International Conference on Micro Electro Mechanical Systems (MEMS) 02/2003. Kyoto, 2003-01-19/23, IEEE, 2003, p.247-250.
20) Isamoto, K.; Totsuka, K.; Suzuki, T.; Sakai, T.; Morosawa, A.; Chong, C.; Fujita, H.; Toshiyoshi, H. 2011 International Conference on Optical MEMS and Nanophotonicstonic. Istanbul, Turkey, 2011-08-8/11. OMN. IEEE, 2011, p.73.
21) Wine, D. W.; Helsel, M. P.; Jenkins, L.; Urey, H.; Osborn, T. D. Proc. SPIE. **4178**, MOEMS and Miniaturized Systems, p.186-196 (2000)
22) Filhol, F.; Defay, E.; Divoux, C.; Zinck, C.; Delaye, M. T. Sens. Actuators A. **123**, p.483-489 (2005)

Trademarks

Development of Technique for Controlling the Nano-order Structure of Anodic Aluminum Oxide

Yoshiharu TAGAWA*, Shinya KUROKAWA**, Atsushi MATSUURA*, Yuya MIYAGAWA*, and Hirokazu SAWADA*

Abstract

In our developed surface treatment technology, we deposit multiple different layers by fine-structure surface treatment to maintain the cleanness level of each layer, increase the surface area, improve surface adhesion, and thus achieve longer run length. This time, we applied the principle of our surface treatment technology to the nano structure of anodic aluminum oxide. In the traditional anodic aluminum oxide, the micro-pores are too small to create a photosensitive layer inside the pores and so cannot contribute to surface adhesion. In this study, we resolved this problem by making a fine structure which has larger micro-pores at the top of the layers and smaller micro-pores at the bottom of the layers.

1. Introduction

The printing industry has been supporting the movement for reducing environmental burden by encouraging the introduction of eco-friendly printing systems, including the Green Printing certification system by the Japan Federation of Printing Industries.[1)]

As a printing plate manufacturer, FUJIFILM has developed Computer to Plate (CTP) systems that produce only a small amount of industrial waste (developer waste) and Plate to Plate systems that recycle the aluminum of consumed CTP plates back to their raw materials.

Fig. 1 illustrates one of those environment-friendly systems. We have made efforts to reduce environmental burden in printing via various green activities throughout the life cycle of planographic products.

Among such efforts, we have provided ecological CTP systems, such as the liquid waste-free processless CTP system, Eco & Free System XZ-R, and the XP-series positive thermal CTP plates that can considerably reduce the amount of developer waste by using it in combination with the developer waste reduction system, XR-2000/5000.

In particular, by mounting the plate onto the printing equipment and realizing on-machine developing at the start of printing, we have created a completely processless CTP system with an ultimate environment-friendly design that does not require either alkaline developing or gum processing. Fig. 2 illustrates

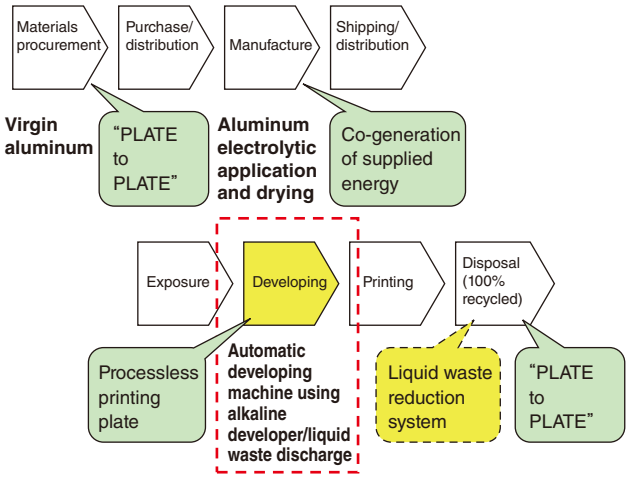

Fig. 1 Example of our environmental conservation efforts.

the stages of the processless CTP system. Different from alkaline developing CTP, neither alkaline developing nor gum processing is necessary; therefore, no associated processing equipment is required, either.[2)]

However, compared with alkaline developing CTP, that ultimate eco-oriented-design, processless CTP plate XZ-R needed further improvements in its printing durability. We therefore developed nano-order structure control technology using anodic aluminum oxide to resolve that problem and applied it to the support for the plate.

Original paper (Received December 2, 2013)

* Research & Development Center
Yoshida-Minami Factory
FUJIFILM Corporation
Kawashiri, Yoshida-cho, Haibara-gun, Shizuoka
421-0396, Japan

** Technical Support & Product Development Division #1
FUJIFILM GLOBAL GRAPHIC SYSTEMS Co., Ltd.
Fujifilm Nishiazabu, Minato-ku, Tokyo
106-0031, Japan

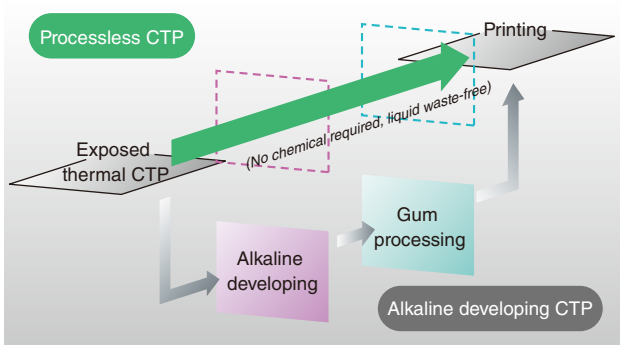

Fig. 2 Process-less CTP system.

2. Characteristics of the support for our processless CTP plates

Fig. 3 illustrates the layer configuration of our processless CTP, XZ-R. The CTP consists of a stratified photosensitive layer, an anodic oxide film and an aluminum support with a relief (grained) structure. The properties required for the support are adhesion to the photosensitive layer for the imaging section and ink detachability, moisture retentivity, hydrophilicity and scratch resistance for the non-imaging section. To improve printing durability, which is of concern, it is necessary to enhance the adhesion of the support to the photosensitive layer without decreasing the functionality of the non-imaging section.

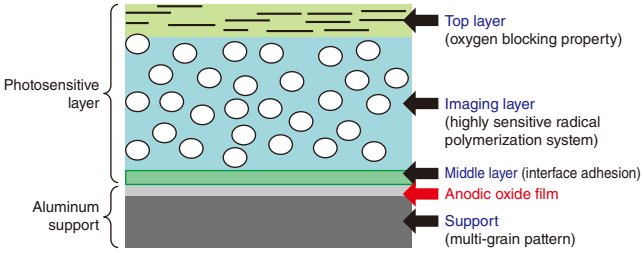

Fig. 3 Configuration of CTP plate (XZ-R).

3. Design policy for the support of our CTP

3.1 Conventional technology

The Multi-Grain V (MGV), which is a support for conventional CTPs, has a relief structure consisting of the following three types of superimposed undulations: (i) large undulations with a wavelength in the order of tens of microns; (ii) medium undulations with a wavelength in the order of microns; and (iii) small undulations with a wavelength of submicron order. Fig. 4 shows the fracture surface structure of the conventional CTP support.

By using those multiple undulations with different wavelengths, it becomes possible to maintain and control the structure of each wavelength, which increases the flexibility of design and improves the balance of physical property values that have a trade-off relationship.

The physical property parameters that may affect the performance of the support are surface area, steepness, arithmetic roughness average (Ra) and density of locally deep parts (Dpn). The surface area has an influence on printing durability and the steepness, on contamination resistance and balance between water and ink. Ra affects printing wetness visibility and Dpn, sensitivity. Fig. 5 illustrates their significance.[3)]

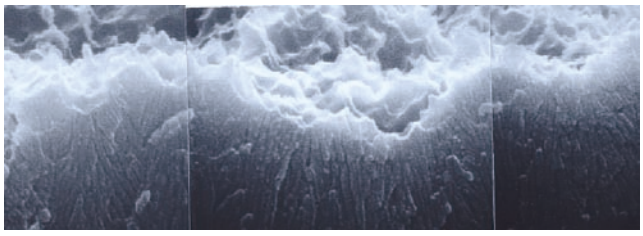

Fig. 4 Cross section of MGV.

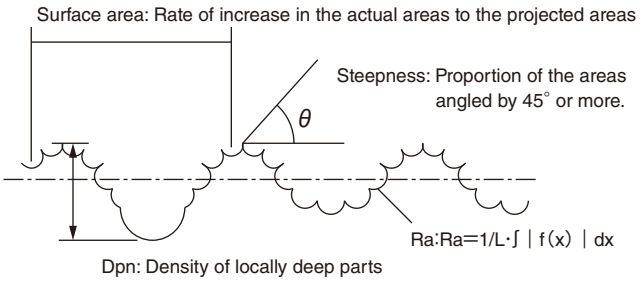

Fig. 5 Physical property parameters of substrate.

The following are the considerations for wavelength design.

(1) Large undulations

Enhancing the retention of dampening solution improves printing wetness visibility. The retention can be improved by increasing Ra. However, if it becomes too large, the unevenness of the photosensitive layer thickness increases, which has an impact on sensitivity. Reducing Dpn realizes an even dispersion of large undulations.

(2) Medium undulations

Medium undulations contribute to contamination resistance and balance between water and ink. Reducing their steepness prevents the retention of ink, which achieves a contamination-resistant support. However, at the same time, that decreases the surface area and affects the adhesion of the support to the photosensitive layer. Thus, printing durability decreases. That is, in optimization, there is a trade-off between contamination resistance and printing durability.

(3) Small undulations

Small undulations with a wavelength of submicron order do not affect contamination resistance. By superimposing those small undulations on medium ones with reduced steepness, low steepness and a larger surface area become compatible. That has achieved the cancellation of the trade-off between contamination resistance and printing durability.

3.2 New nano-order structure controlling technology

Conventional processless CTP uses an MGV support consisting of three sizes of undulations: large, medium and small. To improve the printing durability of our processless CTP by modifying the support design, we have developed a new technology to control the nano-order structure of the anodic oxide film. Specifically, we have improved an idea that has already been employed in the development of supports that have acquired a larger surface area and low steepness by superimposing short-wavelength undulations on longer-wavelength ones.

First, we considered forming a relief structure of undulations with a shorter wavelength than submicron order, applying conventional design principles of supports. To do so, we decided to use micropores, which are nano-order fine structures of the anodic oxide film originally intended to have scratch resistance. Fig. 6 illustrates the wavelengths of the conventional large, medium and small undulations and the micropore diameter of the anodic oxide film.

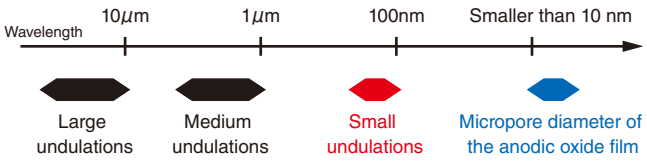

Fig. 6 Size of each wave.

However, micropores at the surface layer of the anodic oxide film have small diameters between 5 and 10 nm and thus the photosensitive layer cannot conform to them. We then enlarged the micropores to make the layer to conform to them, but that resulted in a significant problem. That is, although the intended effect was achieved, the layer sank deep inside the micropores, which substantially decreased on-machine developability. Moreover, even if on-machine development was possible, the non-imaging section became prone to contamination during printing because ink got inside the enlarged micropores.

Fig. 7 provides conceptual images indicating the structural models of anodic oxide films: one having conventional micropores with a surface layer diameter between 5 and 10 nm; and the other having those with a surface layer diameter enlarged to over 10nm.

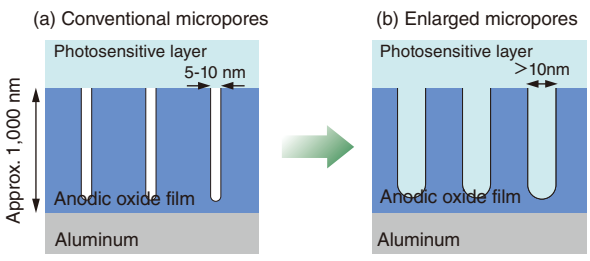

Fig. 7 Anodic aluminum oxide and pore widening.

To resolve that problem, we developed a technology to control the nano-order structure of the anodic oxide film and created one with a stratified structure consisting of larger-diameter pores (top layer) and small-diameter pores (bottom layer). Fig. 8 provides a conceptual image of a stratified anodic oxide film.

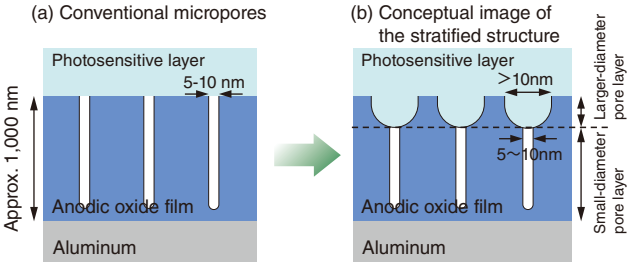

Fig. 8 Configuration of new micro-pores.

Near the surface, the photosensitive layer conforms to the inside of the larger-diameter pores, which enlarges the surface area of the film adhering to that layer. Thus, the film gains improved printing durability. On the other hand, in the bottom layer, the diameter of the pores is so small that the photosensitive layer and ink cannot infiltrate into the pores. That stratified structure improves printing durability without reducing developability or contamination resistance.

Furthermore, the structure does not change the forms of the large, medium and small undulations. Therefore, it is possible to increase the surface area while retaining the characteristics of the conventional support, in particular, steepness. Fig. 9 presents electron micrographs of the surface of a conventional support and the newly developed support. The latter images indicate that the larger-diameter pore layer was formed on the new support without changing the forms of any types of undulations.

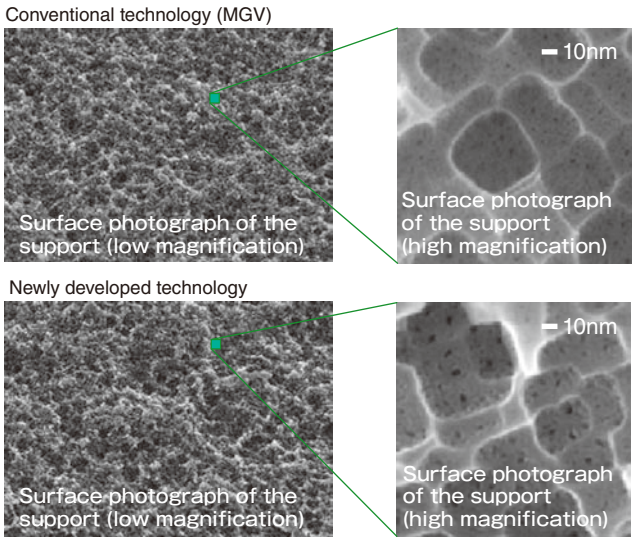

Fig. 9 Surface configuration of MGV and new one.

Fig. 10 shows the relationship between the surface area and the steepness of the medium undulations that affects contamination resistance. It revealed that the new support can achieve a larger surface area than the conventional support with the same steepness.

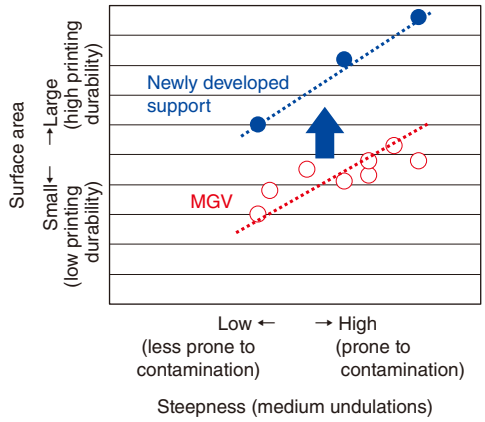

Fig. 10 Steepness and surface area.

3.3 Performance of processless CTP

The results of a performance evaluation with our developed processless CTP sensitive materials confirmed that they can increase printing durability while maintaining the essential performance properties of processless CTP: on-machine developability and contamination resistance (Table 1).

We have thus obtained a prospect for the industrial feasibility of this technology.

Table 1 Performance of new plate.

	Newly developed support	MGV
Exposure sensitivity	120mJ/cm^2	120mJ/cm^2
Printing durability (index)	150	100
On-machine developability	○	○
Contamination resistance	○	○

4. Conclusion

We developed a technology to control the nano-order structure of an anodic aluminum oxide film that is applicable to CTP supports. The technology enables:

- the creation of a stratified anodic oxide film with nano-order micropores consisting of a larger-diameter pore layer and a small-diameter pore layer;
- the improvement of printing durability by increasing the surface area of the top, larger-diameter pore layer of the film adhering to the photosensitive layer; and
- the retention of developability and contamination resistance by the lower, small-diameter pore layer preventing the photosensitive layer and ink from infiltrating into the bottom of the micropore layer.

Applying this technology to processless CTP substantially improves printing durability while retaining on-machine developability and contamination resistance.

We believe that, with this technology, we can contribute even more to the movement for environmental friendliness in the printing market.

References

1) Watanabe, T. Preprints of the 130th JSPST Fall Conference. The Japanese Society of Printing Science and Technology. 2013, A-02.
2) Mori, T. Preprints of the 125th JSPST Spring Conference. The Japanese Society of Printing Science and Technology. 2012, A-04.
3) Oda, A. Preprints of the 111th JSPST Fall Conference. The Japanese Society of Printing Science and Technology. 2003, A-17.

Development of Novel Fluorine-containing Multifunctional Acrylic Monomer

Masayuki HARADA*, Takayuki ITO*, Naoya ISHIDA*, Taiji KATSUMATA*, and Hiroyuki SUZUKI*

Abstract

A highly fluorinated multifunctional acrylic monomer has been developed. The monomer exhibits a low refractive index (n = 1.388), and provides polymers with high crosslink density. In spite of its high fluorine content (44.9 wt%), the monomer easily dissolves in various organic solvents.

1. Introduction

Liquid crystal displays are thin, light and energy-saving. Therefore, their use has been expanded from PC monitors to TVs. In recent years, they have even been introduced into mobile information devices, such as cellular phones, smartphones and tablet PCs, and have thus increased their presence in our daily lives. That recent trend has caused them to require the following surface properties: inhibition of reflection from external light (low reflectivity); resistance to fingerprint adhesion in the case of touch panel usage (contamination resistance); and prevention of damage by scratches (scratch resistance). Currently, to respond to those needs, material development activities have been conducted vigorously. An effective method to realize the above described properties is the introduction of a low refractive-index, low surface-energy fluorine compound to a constituent material of films.[1)] To bestow scratch resistance, a method utilizing a crosslinking reaction during film deposition is often employed. In that case, it is preferable to undertake a curing process after the solution deposition of the films using fluorinated materials with multiple polymerizable groups. To achieve low reflectivity and high contamination resistance, it is effective to employ a compound design that involves an increase of fluorine atom content in the material. However, it is widely known that, as the fluorine content is increased, solubility in general solvents significantly decreases and solution deposition becomes difficult. In addition, that also decreases compatibility with other co-existing materials, which easily causes phase separation of additives and results in a few problems, such as the reduction of film transparency and the inhibition of the expression of intended properties. To solve those problems, we developed a new fluorinated multifunctional acrylic monomer that dissolves easily in general solvents while having a high fluorine content. This paper describes the details of that material.

2. Compound design and synthesis

In the development of a new fluorine compound, we determined the following three requirements for the expression of the intended surface properties of the film.

(i) Having high fluorine content
(ii) Excellent in solvent solubility and not susceptible to the phase separation with other co-existing additives
(iii) Having high curing performance (capable of providing cured products with a high degree of hardness)

As already described, it is known that there is a trade-off relationship between requirements (i) and (ii). In addition, from knowledge gained via consideration of conventional hard coating materials, it is necessary to introduce polymerizable groups each having at least three functional groups in order to fulfill requirement (iii). As a fluorine compound available on the market, Compound 1 whose structure is shown in Fig. 1 is known.[2)] Compound 1 has a high fluorine content (44.3 wt%) and multiple polymerizable groups. However, in the course of examination, we came to conclusion that it does not, at the same time and to the extent we expected, fulfill all the requirements listed above. In particular, with regard to requirement (ii), it was revealed that the compound prevents other co-existing additives from expressing their properties. Evidently, its compatibility with other materials needs improvement. We assumed that phase separation was caused with other additive materials that are non-fluorine compounds because

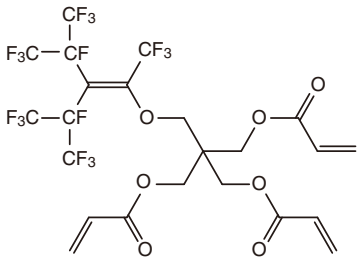

Compound 1

Fig. 1 Commercially available fluorine-containing compound 1.

Original paper (Received December 10, 2013)
*Synthetic Organic Chemistry Laboratories
Research & Development Management Headquarters
FUJIFILM Corporation
Nakanuma, Minamiashigara, Kanagawa
250-0193, Japan

Compound 1 has a molecular structure in which the subunits that contain substituent fluorine atoms are distributed unevenly on the surface of the molecule. To resolve that problem, we invented a molecular design concept shown in Fig. 2 so that those substructures are not located on the molecular surface.

In the molecular design concept (Fig. 2), a molecule is divided into two parts: the core part and the surrounding part. The former contains multiple substituent fluorine atoms and thus the fluorine content of the molecule is increased. On the other hand, hydrocarbon groups are positioned evenly in the latter so that they enclose, inside the molecule, the unevenly distributed substructures having fluorine atoms. In that way, we intended to bestow on Compound 1 compatibility with general organic solvents and co-existing additives that are non-fluorine compounds. Moreover, by introducing multiple polymerizable groups (e.g., acrylic groups) into hydrocarbon groups deployed in surrounding part, it becomes possible to achieve, at the same time, the high curing performance described in requirement (iii).

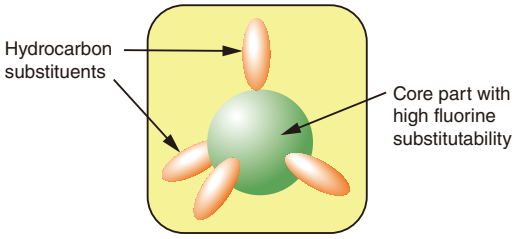

Fig. 2 Design concept of new fluorine compounds.

To design the details of a new compound based on the above concept, we carried out research on the fluorine compounds available on the market that might be suitable for the material of the core part. However, we could not find any such compound among existing ones. We therefore started to design from the very molecular framework of that part.

Assuming that multiple polymerizable groups are finally introduced, we selected polyalcohol as a starting material and formed a core part with a high fluorine content via perfluorination reaction after appropriate linking groups (L) were introduced by applying the usual organic synthesis reaction. Subsequently, we planned to deploy acrylic groups at the end parts (Fig. 3).

For the polyalcohol, we selected three options; trivalent trimethylolethane (TME), tetravalent pentaerythritol (PE) and hexavalent dipentaerythritol (DPE). The longer the chain, the more the linking group (L in Fig. 3) contributes to fluorine atom content after perfluorination reaction. However, shorter chains are rather advantageous for a network structure after a polymerization reaction because the density of crosslinking points becomes higher, helping cured products to be even stronger. Therefore, we set the number of carbon atoms in each straight linking chain to be up to four. By using those three options for the polyalcohol and the linking units, we calculated on paper the fluorine content, the polymerizable group (acrylic group) content and the number of binding sites for crosslinking points of the final product obtained via the scheme presented in Fig. 3. Table 1 summarizes the results.

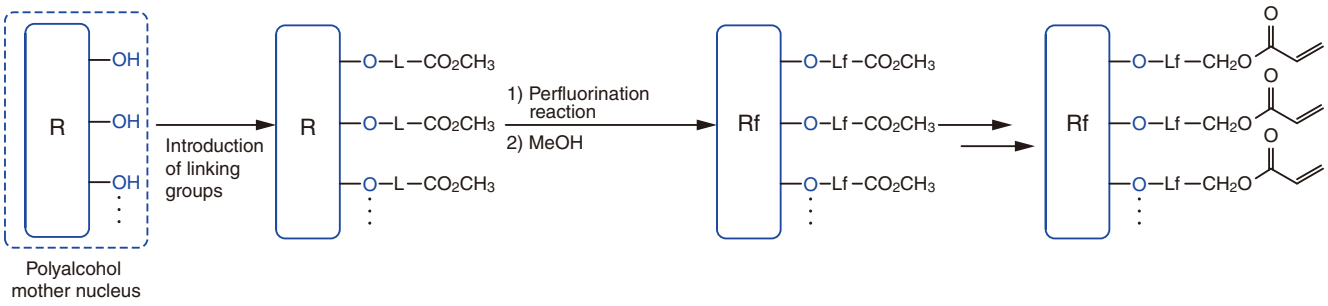

Fig. 3 Synthesis concept of new fluorine compounds.

Table 1 Calculated properties of designed fluorine compounds.

		— CF_2 — (L1)	— $(CF_2)_2$ — (L2)	— $(CF_2)_3$ — (L3)	— $(CF_2)_4$ — (L4)
Fluorine content of the final product (wt%)	TME	41.6	47.8	52.1	55.3
	PE	37.2	44.9	50.0	53.6
	DPE	39.5	46.2	50.8	54.1
Polymerizable group content of the final product*1 (mmol/g)	TME	4.38	3.60	3.05	2.64
	PE	4.90	3.94	3.29	2.82
	DPE	4.46	3.64	3.08	2.67
Number of binding sites for crosslinking points of the final product*2		7	8	9	10
Raw material availability		○	○	△	△
Synthesis suitability		△	○	×~△	×~△

*1: The mmol quantity of acrylic substituents contained per gram of the compound
*2: The number of binding sites between the carbon atoms as the reactive sites of acrylic groups and the crosslinking points inside the molecule (carbon atoms with a molecular chain that diverges into three or four branches)

○ : Good
△ : Medium
× : Not good

As shown in Table 1, the larger the number of carbon atoms in the chain, the higher the fluorine content becomes. At the same time, the polymerizable group content decreases and the number of binding sites for crosslinking points increases. Based on the preferable fluorine content, the lower limit of the polymerizable group content, material availability and synthesis suitability obtained via our considerations thus far, we decided to use L2-type compounds, each of which has two carbon atoms, as the linking group.

We synthesized Compounds 2 to 4 as fluorinated multifunctional compounds having L2-type linking groups (Fig. 4). Among them, the synthesis scheme for Compound 3 is shown in Fig. 5. Compound 3 was obtained in three steps from Compound 5 (total yield: 90%). It is a light yellow, viscous oily substance. The structure was identified with ^{1}H NMR, ^{19}F NMR and MALDI-MS.

Compound 5 was synthesized using pentaerythritol as a starting material according to a method presented in existing literature[3], in which we utilized the liquid-phase fluorination method to cause a perfluorination reaction to substitute all the carbon-hydrogen bonds with fluorine atoms.[4] Among the perfluorination reactions known are electrochemical fluorination, liquid-phase fluorination and vapor-phase fluorination. The electrochemical fluorination reaction is suitable for the fluorination of high-polarity compounds because it is performed in anhydrous hydrofluoric acid. It is subject to bond cleavage, rebonding and isomerization and is often inferior in yield and purity. In the vapor-phase fluorination reaction, the control of heat generation is difficult and the reaction is subject to carbon-carbon bond cleavage. It is also inferior in yield and purity. On the other hand, the liquid-phase fluorination reaction has severe restrictions about reaction solvents (perfluoro solvents) and is difficult to control because it proceeds with radical chains. However, the reaction allows highly flexible molecular design and the intended product can be obtained in relatively high yield and purity. We thus selected that reaction method.

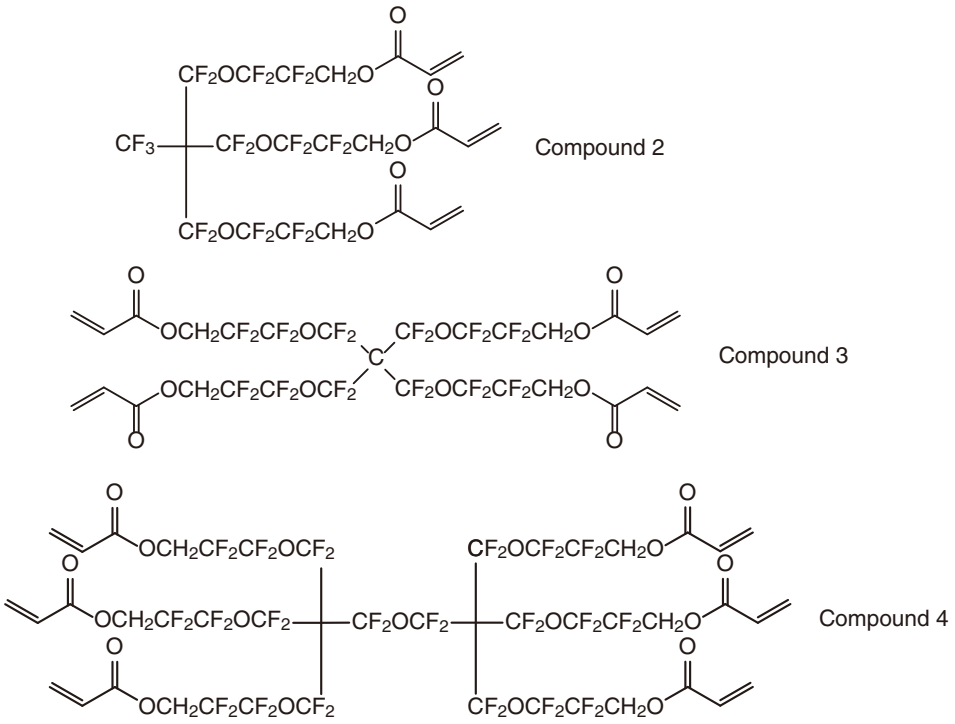

Fig. 4 Synthesized acrylic monomers containing fluorine atoms.

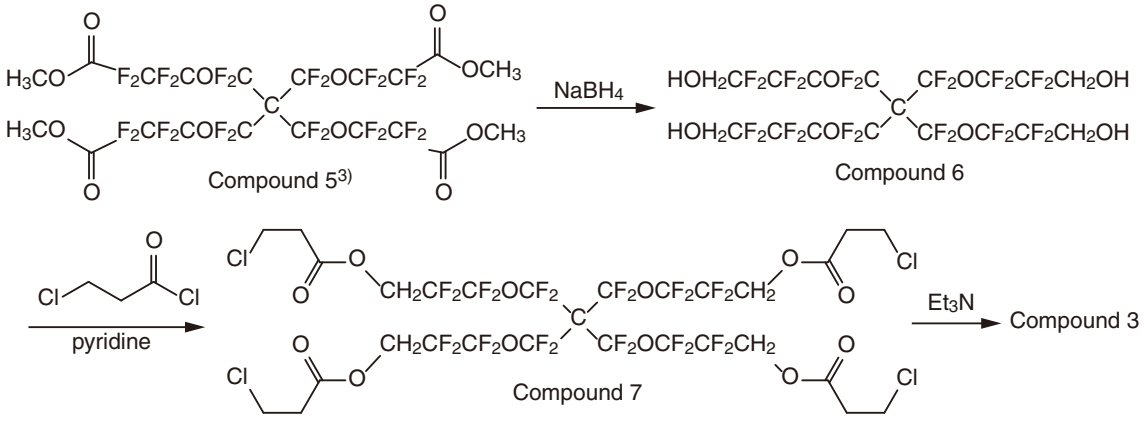

Fig. 5 Synthesis scheme of compound 3.

3. Physical property evaluation

The physical property evaluation of Compounds 2 to 4 above revealed that they were all equally excellent in solubility in general solvents. The relative hardness of their cured films was in the order Compound 3 and Compound 4 (equally best), then Compound 2; and their synthesis suitability (ease of refinement) was ranked Compound 2 and Compound 3 (equally best), then Compound 4. It was thus confirmed that Compound 3 can achieve high performance in all those properties in a well-balanced way.

We compared the physical properties of Compound 3, which was the best in its balance of solubility, hardness and synthesis suitability, and its cured product, with those of a reagent available on the market, 1,6-Bis(acryloyloxy)-2,2,3,3,4,4,5,5-octafluorohexane (Compound 8, Tokyo Chemical Industry, Co., Ltd.) (Table 2). The fluorine content of Compound 3 was 44.9 wt% and higher than that of Compound 8. Accordingly, the refractive indexes of Compound 3 and its cured product were smaller. With regard to microhardness, Compound 3 exhibited a higher value, which was considered to have happened because the compound had more crosslinkable groups and fewer binding sites for crosslinking points and that increased the density of the crosslink structure of the cured product.

Table 3 shows the results of the detailed evaluation for the solvent solubility of Compound 3. Only about 1% of it was dissolved by n-hexane (very small SP value) and methanol (very large SP value). However, it exhibited very high solubility in other general solvents, such as ethyl acetate and methyl ethyl ketone, causing no phase separation even at a concentration of 50 wt%. That means, its high solubility enables easy handling as a coating solution and rarely causes phase separation with the co-existing additives in the composition. That characteristic of Compound 3 can be considered as highly advantageous for optical use that requires high transparency and homogeneity.

Table 2 Chemical and physical properties of compound 3 and 8.

	Compound 3	Compound 8
Appearance	Light yellow transparent liquid	Colorless transparent liquid
Fluorine content	44.9wt%	41.1wt%
Refractive index	Monomer: 1.388 Cured product*: 1.410	Monomer: 1.390 Cured product*: 1.420
Number of binding sites for crosslinking points	8	11
Number of crosslinkable groups	4	2
Contact angle	91.8° (water) 66.8° (CH_2I_2)	74.9° (water) 36.5° (CH_2I_2)
Abbe number*	Monomer: 54.6 Cured product*: 58.0	Monomer: 55.7 Cured product*: 60.0
Microhardness*	136N/mm^2	112N/mm^2

* Cured product:Created from Compound 3 or 8 (containing DAROCUR® 1173 at 1 wt%) onto which high-pressure mercury light (1,000 mJ/cm^2) was irradiated at room temperature under a nitrogen atmosphere after its application to a glass substrate.

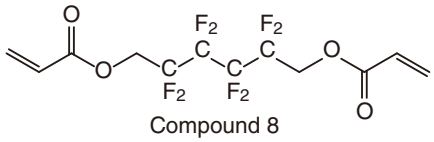

Compound 8

4. Conclusion

The new fluorinated multifunctional acrylic monomer we developed in this research has the following advantageous characteristics compared with conventional compounds: (i) high fluorine content; (ii) high solubility in general organic solvents; and (iii) formability of a dense crosslink structure with four polymerizable groups. Those characteristics make it possible to form low-refractivity and low surface-energy materials with high hardness. It is expected that the compound will not only be utilized for optical films but also developed into a variety of products such as surface coating agents, lens materials and nanoimprint materials.

Table 3 Solubility of compound 3 in common organic solvents.

Solvent	SP value	Solubility at each solid content concentration				
		1wt%	5wt%	10wt%	20wt%	50wt%
n- hexane	7.3	○	×	×	×	×
Toluene	8.8	○	○	○	○	○
Ethyl acetate	9	○	○	○	○	○
Methyl ethyl ketone	9.3	○	○	○	○	○
Acetone	10	○	○	○	○	○
Isopropyl alcohol	11.5	○	○	○	○	○
Methanol	14.5	○	△	△	×	×

○ : Good
△ : Medium
× : Not good

References

1) Yamabe, M., ed. Hussokei-Zairyo No Oyogizyutu(Application of Fluoro Functional Materials). CMC Publishing Co., Ltd., 2006, 350p.
2) Kyoeisha Chemical Co., Ltd. Kinugawa, M., Perfluoro Group-Containing (Meth)Acrylate. JP 2003-313242. 2003-11-06.
3) Felling, Kyle W.; Youngstrom, Cameron R.; Lagow, Richard J. Journal of Fluorine Chemistry, 2004, **125** (5), p.749-754 (2004)
4) (a) Exfluor Research Corporation. Bierschenk, Thomas R.; Juhlke, Timothy; Kawa, Hajimu; Lagow, Richard J. Liquid phase fluorination. US 5,093,432 A. 1992-03-03.
(b) Okazoe, T.; Watanabe, K.; Itoh, M.; Shirakawa, D.;Murofushi, H.; Okamoto, H.; Tatematsu, S. Advanced Synthesis & Catalysis **343** (2), p.215-219 (2001)

Editorial Note

On January 20, 2014, FUJIFILM Corporation commemorated the 80th anniversary of its foundation. To mark the occasion, the company published a brand statement and created a new corporate slogan, "Value from Innovation," declaring its mission to keep creating value for customers. In addition, aiming at *co-creation* using external technology in combination with its own, the company set up the Open Innovation Hub on the second floor of the Tokyo Midtown West building, thus entering a new era for the next few decades.

This annual journal reviews the results of our research and development. It consists of original papers describing our new products and technologies and those reproduced from recently published science and technology journals. For this issue, ten original papers and fourteen reproduced ones were selected mainly from the fields of medical/healthcare products and ink jet technology in which we have made great progress in the last year. Many other research products are expected to be commercialized soon, and articles about those technologies will appear from the next issue onward.

I hope this journal will assist our R&D activities and new business creation projects based on the concept of *co-creation*.

Toshiaki Aoai
Editor in Chief